TU Delft

Delft University of Technology

Connecting central carbon and aromatic amino acid metabolisms to improve de novo 2-phenylethanol production in Saccharomyces cerevisiae

Hassing, Else Jasmijn; de Groot, Philip A.; Marquenie, Vita R.; Pronk, Jack T.; Daran, Jean Marc G.

DOI
10.1016/j.ymben.2019.09.011

Publication date
2019

Document Version
Final published version

Published in
Metabolic Engineering

Citation (APA)
Hassing, E. J., de Groot, P. A., Marquenie, V. R., Pronk, J. T., & Daran, J. M. G. (2019). Connecting central carbon and aromatic amino acid metabolisms to improve de novo 2-phenylethanol production in Saccharomyces cerevisiae. *Metabolic Engineering*, *56*, 165-180. https://doi.org/10.1016/j.ymben.2019.09.011

Important note
To cite this publication, please use the final published version (if applicable).
Please check the document version above.

Copyright
Other than for strictly personal use, it is not permitted to download, forward or distribute the text or part of it, without the consent of the author(s) and/or copyright holder(s), unless the work is under an open content license such as Creative Commons.

Takedown policy
Please contact us and provide details if you believe this document breaches copyrights.
We will remove access to the work immediately and investigate your claim.

This work is downloaded from Delft University of Technology.
For technical reasons the number of authors shown on this cover page is limited to a maximum of 10.

Metabolic Engineering 56 (2019) 165–180

Contents lists available at ScienceDirect

Metabolic Engineering

journal homepage: www.elsevier.com/locate/meteng

Connecting central carbon and aromatic amino acid metabolisms to improve *de novo* 2-phenylethanol production in *Saccharomyces cerevisiae*

Else-Jasmijn Hassing, Philip A. de Groot, Vita R. Marquenie, Jack T. Pronk, Jean-Marc G. Daran*

Department of Biotechnology, Delft University of Technology, Van der Maasweg 9, 2629 HZ, Delft, the Netherlands

ARTICLE INFO

Keywords:
2-Phenylethanol
de novo biosynthesis
Saccharomyces cerevisiae
Aromatic amino acid pathway engineering
Prephenate dehydrogenase downregulation
Pyruvate kinase

ABSTRACT

The organic compound 2-phenylethanol (2PE) has a pleasant floral scent and is intensively used in the cosmetic and food industries. Microbial production of 2PE by phenylalanine bioconversion or *de novo* biosynthesis from sugar offer sustainable, reliable and natural production processes compared to chemical synthesis. Despite the ability of *Saccharomyces cerevisiae* to naturally synthesize 2PE, *de novo* synthesis in high concentration and yield remains a metabolic engineering challenge. Here, we demonstrate that improving phosphoenolpyruvate supply by expressing pyruvate kinase variants and eliminating the formation of *p*-hydroxy-phenylethanol without creating tyrosine auxotrophy significantly contributed to improve 2PE production in *S. cerevisiae*. In combination with the engineering of the aromatic amino acid biosynthesis and Ehrlich pathway, these mutations enabled better connection between glycolysis and pentose phosphate pathway optimizing carbon flux towards 2PE. However, attempts to further connect these two parts of central carbon metabolism by redirecting fructose-6P towards erythrose-4P by expressing a phosphoketolase-phosphotransacetylase pathway did not result in improved performance. The best performing strains were capable of producing 13mM of 2PE at a yield of 0.113 mol mol^{-1}, which represents the highest yield for *de novo* produced 2PE in *S. cerevisiae* and other yeast species.

1. Introduction

Flavourings and fragrances compounds are used in a wide range of application sectors including food, beverage, cosmetic and perfume industries. The organic compound 2-phenylethanol (2PE) is characterized by a pleasant fresh rose and green phenolic muguet scent. Additionally, 2PE serves as a building block for other products such as phenylethyl acetate, a flavouring agent with rose, honey and raspberry notes (Etschmann et al., 2002).

Although the most cost effective 2PE production processes are based on chemical synthesis, these methods are gradually replaced by biological production processes. The absence of substrate stereo-selectivity of the 2PE chemical synthesis processes leads to formation of by-products that require use of non-environmentally friendly purification steps. Additionally, the European and US regulations restricted food grade 2PE to natural sources which in this case includes botanical and microbiological sources, comprising fermentation products (The_european_parliament_and_the_council_of_the_European_union, 2008). The first 2PE natural source derives from plant and flower essential oils extraction, mostly rose petals (Xu et al., 2007). However, this supply is limited and impeded by costs of purification (Eikani et al., 2005; Kim et al., 2014; Longo and Sanromán, 2006). The second 2PE natural source is the product of microbial metabolism. 2PE is the product of the Ehrlich pathway (Ehrlich, 1907). Several amino acids (branched-chain and aromatic amino acids as well as methionine) can be assimilated by the Ehrlich pathway and converted in higher fusel alcohols. The pathway consists of three reactions, i) a transamination of the amino acid, ii) a decarboxylation of the 2-oxo acid formed in the preceding reaction and iii) a reduction of the resulting fusel aldehyde into the higher fusel alcohol (Hazelwood et al., 2008). The yeast *Saccharomyces cerevisiae,* traditionally used in wine, beer and bread fermentation naturally produces, next to ethanol and CO_2, a range of higher alcohols and esters which have a strong impact on the sensory properties and quality of the products (Cordente et al., 2019; Liu et al., 2018). This characteristic has been exploited to produce 2PE from phenylalanine by whole-cell bioconversion (Eshkol et al., 2009; Etschmann and Schrader, 2006; Stark et al., 2002, 2003). However, biotransformation often relies on multi-stages approaches, adding-up operation units and use of substrate precursor that on the long term might limit the attractiveness of this method. *De novo* 2PE production

* Corresponding author. Van der Maasweg 9, 2629HZ, Delft, the Netherlands.
E-mail addresses: E.Hassing@tudelft.nl (E.-J. Hassing), padgroot@gmail.com (P.A. de Groot), V.R.Marquenie@student.tudelft.nl (V.R. Marquenie), J.T.Pronk@tudelft.nl (J.T. Pronk), J.G.Daran@tudelft.nl (J.-M.G. Daran).

https://doi.org/10.1016/j.ymben.2019.09.011
Received 20 July 2019; Received in revised form 25 September 2019; Accepted 25 September 2019
Available online 28 September 2019
1096-7176/ © 2019 Published by Elsevier Inc. on behalf of International Metabolic Engineering Society.

Abbreviations

FBR	Feedback resistant allele
Glc	glucose
G6P	glucose-6-phosphate
F6P	fructose-6-phosphate
AcP	acetyl-P
ACE	acetate
AcCOA	acetyl-coA
TCA	tricarboxylic acid cycle
PYR	pyruvate
PEP	phosphoenolpyruvate
E4P	erythose-4-phosphate
DAHP	3-deoxy-D-arabino-heptulosonate-7-phosphate
CHR	chorismate
SHK	shikimate
PPA	prephenate
PPY	phenylpyruvate
PHE	L-phenylalanine
PAC	phenylacetaldehyde
PAA	phenylacetate
2PE	2-phenylethanol
*p*OHPPY	p-hydroxyphenylpyruvate
TYR	L-tyrosine
TRP	tryptophan
*p*OHPAC	p-hydroxyphenylacetaldehyde
*p*OHPAA	p-hydroxyphenylacetate
*p*OH2PE	p-hydroxyphenylethanol

using a low cost, renewable sugar such as glucose could represent a promising alternative to phenylalanine bioconversion.

In *S. cerevisiae*, the Ehrlich pathway precursor phenylpyruvate is directly derived from the shikimate pathway. This pathway starts with the condensation of the glycolytic intermediate phosphoenolpyruvate (PEP) and the pentose phosphate pathway intermediate erythrose 4-phospate (E4P) to form the first dedicated metabolite of the shikimate pathway deoxy-d-arabino-heptulosonate-7-phosphate (DAHP). DAHP is then converted to chorismate in six consecutive steps catalysed by the enzymes Aro1-Aro4 and Aro7 (Ball et al., 1986; Duncan et al., 1988; Helmstaedt et al., 2005; Jones et al., 1991). Chorismate is the last common intermediate of all three aromatic amino acids. There, the pathway divides in two branches, one towards tryptophan (TRP) and the other towards phenylalanine (PHE) and tyrosine (TYR). The latter branch is catalysed by the chorismate mutase Aro7. The product of this reaction, prephenate (PPA), is then either directed to the 2-oxo acid phenylpyruvate (PPY) or to *p*-hydroxyphenylpyruvate (*p*OHPPY) catalysed by the prephenate dehydratase *PHA2* or the prephenate dehydrogenase *TYR1,* respectively. The 2-oxo acids can then be transaminated to phenylalanine or tyrosine by the aromatic amino acid transferases I (Aro8) or II (Aro9) depending on the nitrogen source (Iraqui et al., 1998, 1999). Alternatively, the resulting 2-oxo acid can get decarboxylated by a phenylpyruvate decarboxylase into a fusel aldehyde (Boer et al., 2007; Vuralhan et al., 2005). In *S. cerevisiae*, this step is mainly catalysed by the thiamine pyrophosphate (TPP)-dependent 2-oxo acid decarboxylase, Aro10 (Romagnoli et al., 2012; Vuralhan et al., 2003). Finally, fusel aldehydes can either be reduced to fusel alcohols (Dickinson et al., 2003) or oxidized to a fusel acids depending on the redox status of the cells (Vuralhan et al., 2005) (Fig. 1).

Hitherto, pathway engineering strategies for *de novo* production of

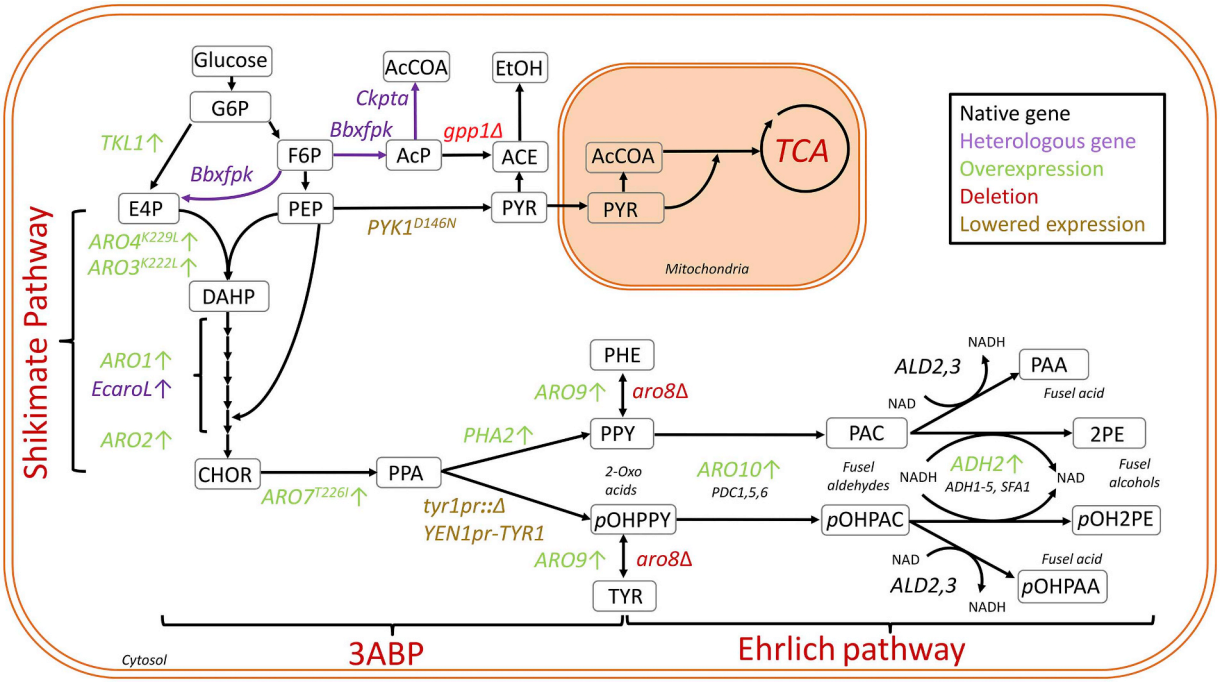

Fig. 1. Adapted metabolic pathway for increased 2PE production in *S. cerevisiae*. Native enzymatic pathways are indicated with black arrows. Heterologous enzymatic pathways are indicated in purple. Overexpressed genes are highlighted in green, deleted genes are annotated in red, genes with lowered expression are shown in brown and heterologous enzymes are depicted in purple.

FBR Feedback resistant allele, Glc glucose, G6P glucose-6-phosphate, F6P fructose-6-phosphate, AcP acetyl-P, ACE acetate, AcCOA acetyl-coA, TCA tricarboxylic acid cycle, PYR pyruvate, PEP phosphoenolpyruvate, E4P erythose-4-phosphate, DAHP 3-deoxy-D-arabino-heptulosonate-7-phosphate, CHR chorismate, PPA prephenate, PPY phenylpyruvate, PHE L-phenylalanine, PAC phenylacetaldehyde, PAA phenylacetate, 2PE

2-phenylethanol, *p*OHPPY *p*-hydroxyphenylpyruvate, *TYR* L-tyrosine, *p*OHPAC *p*-hydroxyphenylacetaldehyde, *p*OHPAA p-hydroxyphenylacetate, *p*OH2PE *p*-hydroxyphenylethanol. (For interpretation of the references to colour in this figure legend, the reader is referred to the Web version of this article.)

2PE essentially targeted the shikimate and the Ehrlich pathways (Wang et al., 2019). In the case of aromatic amino acids, the DAHP synthases Aro3 and Aro4, are feedback inhibited by phenylalanine and tyrosine, respectively (Helmstaedt et al., 2005; Luttik et al., 2008) and the chorismate mutase Aro7 is allosterically controlled by tyrosine and tryptophan that act as an inhibitor or activator, respectively (Helmstaedt et al., 2002; Schnappauf et al., 1998a, 1998b). Expression of a DAHP synthase allele encoding a feedback insensitive variant (*ARO4*^{K229L}) in *S. cerevisiae* was shown to be sufficient to yield *de novo* synthesis of aromatic amino acid derived Ehrlich metabolites (Luttik et al., 2008). Co-expression of alleles encoding both Aro4^{K229L} and Aro3^{K222L} feedback insensitive variants further improved production of metabolites derived from the shikimate pathway (Reifenrath et al., 2018). In contrast to the DAHP synthase, the sole alleviation of the feedback inhibition of Aro7 showed no impact on the formation of Ehrlich metabolites. However, the combined expression of these variant alleles promoted a significant 4-fold increase of the flux through the aromatic amino acid pathway yielding a 200-fold increase of extracellular concentration of the aromatic Ehrlich metabolites and improved fusel alcohol production (Luttik et al., 2008). Although previously applied engineering strategies significantly increased 2PE biosynthesis (0.41 g L^{-1}, yield of 0.03 mol 2PE per mol glucose consumed), the product yields achieved are still one order of magnitude lower than the calculated glucose maximum theoretical yield (0.500 mol mol^{-1}).

The aim of this study was to define a metabolic engineering strategy to improve *de novo* production of 2PE by *S. cerevisiae*, using glucose as sole carbon source. To do so, central carbon metabolism was modified to optimize supply of E4P and PEP to the shikimate pathway. This was combined with the overexpression and mutations alleviating allosteric regulation of genes of the shikimate and Ehrlich pathways. In addition the flux towards by-products was decreased by down-tuning transcriptional regulation of competing metabolic branches (Fig. 1).

2. Material and methods

2.1. Strains and culture conditions

All yeast strains used in this study belong to the CEN.PK lineage (Entian and Kötter, 2007) (Table 1). Strains were grown in 500 mL shake flasks containing 100 mL complex medium (YPD) with 10 g L^{-1} Bacto Peptone, 20 g L^{-1} glucose and 200 mg L^{-1} hygromycin or 100 mg L^{-1} nourseothricin when required. Alternatively, strains were grown in chemically defined (synthetic) medium (SM) containing 3 g L^{-1} KH_2PO4, 0.5 g L^{-1} $MgSO_4{\cdot}7H_2O$, 5 g L^{-1} $(NH_4)_2SO_4$, 1 mL L^{-1} trace element solution and 1 mL L^{-1} vitamin solution (Verduyn et al., 1992) containing 20 g L^{-1} glucose with 150 mg L^{-1} uracil, 76 mg L^{-1} phenylalanine and 225 mg L^{-1} tyrosine when required (Pronk, 2002). Synthetic medium with urea as sole nitrogen source consisted of 3 g L^{-1} KH_2PO_4, 0.5 g L^{-1} $MgSO_4{\cdot}7H_2O$, 5 g L^{-1} K_2SO_4, 2.3 g L^{-1} filter sterilized urea, 1 mL L^{-1} trace element solution and 1 mL L^{-1} vitamin solution containing 20 g L^{-1} glucose and 200 mg L^{-1} hygromycin when required (Luttik et al., 2000). All strains were grown at 30 °C at 200 RPM. Solid medium was obtained by the addition of 2% (w/v) bacto peptone prior to heat sterilization.

Escherichia coli XL1 blue cells (Agilent Technologies, Santa Clara, CA) were used for plasmids storage and propagation. *E. coli* cells were grown in lysogeny broth (LB) with supplementation of 100 mg L^{-1} ampicillin, 25 mg L^{-1} chloramphenicol or 50 mg L^{-1} kanamycin. Solid medium was obtained by the addition of 2% (w/v) bacto peptone prior to heat sterilization.

Yeast and *E. coli* cultures were stored by adding 30% (v/v) glycerol to exponentially growing cells and storing the aliquots at -80 °C.

2.2. Molecular biology techniques

For cloning purposes, Phusion high fidelity polymerase (Thermo Scientific, Landsmeer, Netherlands) was used according to manufacturer's recommendations with the exception that the primer and polymerase concentrations were set at 200 nM and 0.03 μL^{-1} respectively. Genomic DNA used as template for PCR amplification was isolated using the YeaStar genomic DNA kit (Zymo Research, Irvine, CA) according to manufacturer's instructions. PCR products were purified by gel purification using Zymoclean kit (Zymo Research) according to manufacturer's recommendations using milliQ as eluent solvent. Alternatively, PCR products were digested for an hour using 1 μl DpnI FastDigest enzyme (Thermo Fisher Scientific). The digested products were then purified using the GenElute™ PCR clean-Up Kit (Sigma-Aldrich, St. Louis, MO). Diagnostic PCR was performed using DreamTaq PCR mastermix (Thermo Fisher Scientific). A list of diagnostic primers is provided in Table S1. Plasmids were isolated from *E. coli* using the GenElute plasmid miniprep kit (Sigma-Aldrich) according to manufacturer's instructions using miliQ water as eluent.

2.3. Plasmid construction

All constructed plasmids were transformed to *E. coli* (XL1-Blue) cells according to the manufacturer's recommendations and grown under selective conditions. Plasmids used in this study are given in Table S2.

2.3.1. Construction of Cas9 reprogramming gRNA plasmids

Plasmids containing either single or double gRNA for Cas9 targeting of specific loci were constructed as described by Mans et al. (2015).

2.3.2. Construction of the expression cassettes

The construction of promoter, gene or terminator part plasmids compatible with Golden Gate assembly following the yeast tool kit principle (Lee et al., 2015) were constructed by first amplifying the region of interest with primers providing part type specific overhangs and assembling these fragments in either pUD565 (Boonekamp et al., 2018) or pUD564 (Table S2), two GFP dropout entry vectors containing chloramphenicol or kanamycin resistance genes, respectively.

Genomic DNA from *S. cerevisiae* CEN.PK113-7D, *Saccharomyces kudriavzevii* CR85 or *Saccharomyces eubayanus* CBS12357 was used as template DNA for amplifying the promoter regions. Primers providing promoter part type specific overhangs (AACG and CATA) (Table S1) were used to amplify the following fragments: *PDC1*$_p$ (9755 & 9756) *ENO2*$_p$ (9739 & 9740), *PGI1*$_p$ (9630 & 9631), *PYK1*$_p$ (10608 & 10609), *THD3*$_p$ (10753 & 10754), *PGK1*$_p$ (9421 & 9422), *SkADH1*$_p$ (9737 & 9738), *SkTDH3*$_p$ (9751 & 9752), *SkPDC1*$_p$ (9731 & 9732), *SkFBA1*$_p$ (9640 & 9641), *SePDC1*$_p$ (9729 & 9730), *SeFBA1*$_p$ (9409 & 9410) and *SeGPM1*$_p$ (9759 & 9760). Additionally, *ENO2*$_p$ was also ordered synthesized using the GeneArt gene Synthesis (ThermoFisher Scientific) with upstream the promoter specific YeastToolkit flank 'AAGCATCGT CTCATCGGTCTCAAACG' and downstream with 'TTATGCCGTCTCAGG TCTCACATA' (Lee et al., 2015). The promoter fragments were cloned into entry vector pUD565 using BsmBI mediated golden gate assembly resulting in part plasmids pGGKp025 (*PDC1*$_p$), pGGKp028 (*ENO2*$_p$), pGGKp033 (*PGI1*$_p$), pGGKp034 (*PYK1*$_p$), pGGKp035 (*THD3*$_p$), pGGKp036 (*PGKI*$_p$), pGGKp062 (*SkADH1*$_p$) pGGKp063 (*SkTDH3*$_p$), pGGKp064 (*SkPDC1*$_p$), pGGKp065 (*SkFBA1*$_p$), pGGKp074 (*SePDC1*$_p$), pGGKp075 (*SeFBA1*$_p$), pGGKp095 (*SeGPM1*$_p$) and pGGKp164 (*ENO2*$_p$).

Terminator constructs were all obtained from CEN.PK113-7D genomic DNA, this time using terminator part type specific overhang (ATCC and CAGC) primers (Table S1) obtaining fragments *ADH1*$_t$ (10769 & 10770), *TEF2*$_t$ (10884 & 10885), *TEF1*$_t$ (10767 & 10768), *PYK1*$_t$ (10886 & 10887), *TDH3*$_t$ (10761 & 10762), *PDC1*$_t$ (10773 & 10774) and *GPM1*$_t$ (10759 & 10760). Additionally, the *PGI1*$_p$, *PFK1*$_p$

Table 1
Strains used in this study. *Bb Bifidobacterium breve*, *Ck Clostridium kluyveri*, *Ec Escherichia coli*, *Kl Kluyveromyces lactis* and *Sp Streptococcus pyogenes*.

Strain	Relevant genotype	Reference
CEN.PK113-7D	*MATa URA3 HIS3 LEU2 TRP1 MAL2-8c SUC2*	Entian and Kötter (2007)
S.kudriavzevii CR85	*MATa/Matα*	Lopes et al. (2010)
S. eubayanus CBS12357	*MATa/Matα*	Libkind et al. (2011)
IMX581	*ura3-52 can1Δ::Spcas9-natNT2*	Mans et al. (2015)
IME324	*ura3-52 can1Δ::Spcas9-natNT2* p426-TEF *(URA3)*	Papapetridis et al. (2017)
IMN002	*ura3-52 aro3Δ ARO4$_p$-ARO4Δ::TDH3$_p$-ARO4^{K229L}*	Luttik et al. (2008)
IMX1492	*ura3-52 s$_p$3Δ::Spcas9-natNT2 aro3Δ TDH3$_p$-ARO4^{K229L}*	This study
IMX1533	*ura3-52 s$_p$3Δ::Spcas9-natNT2 aro3Δ aro7Δ TDH3$_p$-ARO4^{K229L}*	This study
IMX1586	*ura3-52 spr3Δ::Spcas9-natNT2 aro3Δ aro7Δ TDH3$_p$-ARO4^{K229L} GPM1$_p$-ARO7^{T226I}-TEFt$_t$* pUDR649 (*KlURA3,* gRNA-*ARO7$_p$*)	This study
IMX1593	*ura3-52 spr3Δ::Spcas9-natNT2 aro3Δ aro7Δ TDH3$_p$-ARO4^{K229L} ARO7$_p$::SeGPM1$_p$-ARO7^{T226I}-TEF1t*	This study
IMX1754	*ura3-52 can1Δ::Spcas9-natNT2 aro3Δ* pUDR409 (*KlURA3,* gRNA-*ARO3*)	This study
IMX1783	*ura3-52 can1Δ::Spcas9-natNT2 aro3Δ*	This study
IMX1952	*ura3-52 can1Δ::Spcas9-natNT2 aro3Δ TDH3$_p$-ARO4^{K229L}-ENO2t* shrDA *SkTDH3$_p$-PHA2-TEF2$_t$* shrDB *SePDC1$_p$-ARO2-SSA1t* shrDC *SeFBA1$_p$-ARO9-ADH1t* shrDD *SeGPM1pt-ARO7^{T226I}-TEF1t* shrDE *ENO2$_p$-ARO1*	This study
IMX1955	*ura3-52 can1Δ::Spcas9-natNT2 aro3Δ TDH3$_p$-ARO4^{K229L}-ENO2t* shrDA *SkTDH3$_p$-PHA2-TEF2t* shrDB *SePDC1$_p$-ARO2-SSA1t* shrDC *SeFBA1$_p$-ARO9-ADH1t* shrDD *SeGPM1$_p$-ARO7^{T226I}-TEF1t* shrDE *ENO2$_p$-ARO1 sga1Δ::ENO2$_p$-TKL1-TDH3t* pUDR372 (*klURA3,* gRNA-*SGA1*)	This study
IMX2029	*ura3-52 can1Δ::Spcas9-natNT2 aro3Δ TDH3$_p$-ARO4^{K229L}-ENO2t* shrDA *SkTDH3$_p$-PHA2-TEF2t* shrDB *SePDC1$_p$-ARO2-SSA1t* shrDC *SeFBA1$_p$-ARO9-ADH1t* shrDD *SeGPM1$_p$-ARO7^{T226I}-TEF1t* shrDE *ENO2$_p$-ARO1 sga1Δ::ENO2$_p$-TKL1-TDH3t*	This study
IMX2051	*ura3-52 can1Δ::Spcas9-natNT2 tyr1Δ*	This study
IMX2052	*ura3-52 can1Δ::Spcas9-natNT2 aro3Δ tyr1Δ TDH3$_p$-ARO4^{K229L}-ENO2t* shrDA *SkTDH3$_p$-PHA2-TEF2t* shrDB *SePDC1$_p$-ARO2-SSA1t* shrDC *SeFBA1$_p$-ARO9-ADH1t* shrDD *SeGPM1$_p$-ARO7^{T226I}-TEF1t* shrDE *ENO2$_p$-ARO1 sga1Δ::ENO2$_p$-TKL1-TDH3t*	This study
IMX2056	*ura3-52 can1Δ::Spcas9-natNT2 aro3Δ aro8Δ TDH3$_p$-ARO4^{K229L}-ENO2t* shrDA *SkTDH3$_p$-PHA2-TEF2t* shrDB *SePDC1$_p$-ARO2-SSA1t* shrDC *SeFBA1$_p$-ARO9-ADH1t* shrDD *SeGPM1$_p$-ARO7^{T226I}-TEF1t* shrDE *ENO2$_p$-ARO1 sga1Δ::ENO2$_p$-TKL1-TDH3t*	This study
IMC124	*ura3-52 can1Δ::Spcas9-natNT2 aro3Δ aro8Δ TDH3$_p$-ARO4^{K229L}-ENO2t* shrDA *SkTDH3$_p$-PHA2-TEF2t* shrDB *SePDC1$_p$-ARO2-SSA1t* shrDC *SeFBA1$_p$-ARO9-ADH1t* shrDD *SeGPM1$_p$-ARO7^{T226I}-TEF1t* shrDE *ENO2$_p$-ARO1 sga1Δ::ENO2$_p$-TKL1-TDH3t* pUDC245 (*CEN6/ARS4, URA3, SkPDC1$_p$-EcaroG^{P150L}-ScPFK1t*)	This study
IMC125	*ura3-52 can1Δ::Spcas9-natNT2 aro3Δ aro8Δ TDH3$_p$-ARO4^{K229L}-ENO2t* shrDA *SkTDH3$_p$-PHA2-TEF2t* shrDB *SePDC1$_p$-ARO2-SSA1t* shrDC *SeFBA1$_p$-ARO9-ADH1t* shrDD *SeGPM1$_p$-ARO7^{T226I}-TEF1t* shrDE *ENO2$_p$-ARO1 sga1Δ::ENO2$_p$-TKL1-TDH3t* pUDC246 (*CEN6/ARS4, URA3, SkADH1$_p$-EcaroB-ScFBA1t*)	This study
IMC126	*ura3-52 can1Δ::Spcas9-natNT2 aro3Δ aro8Δ TDH3$_p$-ARO4^{K229L}-ENO2t* shrDA *SkTDH3$_p$-PHA2-TEF2t* shrDB *SePDC1$_p$-ARO2-SSA1t* shrDC *SeFBA1$_p$-ARO9-ADH1t* shrDD *SeGPM1$_p$-ARO7^{T226I}-TEF1t* shrDE *ENO2$_p$-ARO1 sga1Δ::ENO2$_p$-TKL1-TDH3t* pUDC247 (*CEN6/ARS4, URA3, SkFBA1$_p$-EcaroD-TDH3t*)	This study
IMC127	*ura3-52 can1Δ::Spcas9-natNT2 aro3Δ aro8Δ TDH3$_p$-ARO4^{K229L}-ENO2t* shrDA *SkTDH3$_p$-PHA2-TEF2t* shrDB *SePDC1$_p$-ARO2-SSA1t* shrDC *SeFBA1$_p$-ARO9-ADH1t* shrDD *SeGPM1$_p$-ARO7^{T226I}-TEF1t* shrDE *ENO2$_p$-ARO1 sga1Δ::ENO2$_p$-TKL1-TDH3t* pUDC248 (*CEN6/ARS4, URA3, TDH2$_p$-EcaroE-PDC1t*)	This study
IMC128	*ura3-52 can1Δ::Spcas9-natNT2 aro3Δ aro8Δ TDH3$_p$-ARO4^{K229L}-ENO2t* shrDA *SkTDH3$_p$-PHA2-TEF2t* shrDB *SePDC1$_p$-ARO2-SSA1t* shrDC *SeFBA1$_p$-ARO9-ADH1t* shrDD *SeGPM1$_p$-ARO7^{T226I}-TEF1t* shrDE *ENO2$_p$-ARO1 sga1Δ::ENO2$_p$-TKL1-TDH3t* pUDC249 (*CEN6/ARS4, URA3, SePDC1$_p$-EcaroL-ADH3t*)	This study
IMC129	*ura3-52 can1Δ::Spcas9-natNT2 aro3Δ aro8Δ TDH3$_p$-ARO4^{K229L}-ENO2t* shrDA *SkTDH3$_p$-PHA2-TEF2t* shrDB *SePDC1$_p$-ARO2-SSA1t* shrDC *SeFBA1$_p$-ARO9-ADH1t* shrDD *SeGPM1$_p$-ARO7^{T226I}-TEF1t* shrDE *ENO2$_p$-ARO1 sga1Δ::ENO2$_p$-TKL1-TDH3t* pUDC250 (*CEN6/ARS4, URA3, SkFBA1$_p$-EcaroA-PGI1t*)	This study
IMC130	*ura3-52 can1Δ::Spcas9-natNT2 aro3Δ aro8Δ TDH3$_p$-ARO4^{K229L}-ENO2t* shrDA *SkTDH3$_p$-PHA2-TEF2t* shrDB *SePDC1$_p$-ARO2-SSA1t* shrDC *SeFBA1$_p$-ARO9-ADH1t* shrDD *SeGPM1$_p$-ARO7^{T226I}-TEF1t* shrDE *ENO2$_p$-ARO1 sga1Δ::ENO2$_p$-TKL1-TDH3t* pUDC251 (*CEN6/ARS4, URA3, TDH3$_p$-EcaroC-PFK2t*)	This study
IMC131	*ura3-52 can1Δ::Spcas9-natNT2 aro3Δ aro8Δ TDH3$_p$-ARO4^{K229L}-ENO2t* shrDA *SkTDH3$_p$-PHA2-TEF2t* shrDB *SePDC1$_p$-ARO2-SSA1t* shrDC *SeFBA1$_p$-ARO9-ADH1t* shrDD *SeGPM1$_p$-ARO7^{T226I}-TEF1t* shrDE *ENO2$_p$-ARO1 sga1Δ::ENO2$_p$-TKL1-TDH3t* pUDC252 (*CEN6/ARS4, URA3, ENO2$_p$-EcpheA^{T326P}-GPM1t*)	This study
IMC132	*ura3-52 can1Δ::Spcas9-natNT2 aro3Δ aro8Δ TDH3$_p$-ARO4^{K229L}-ENO2t* shrDA *SkTDH3$_p$-PHA2-TEF2t* shrDB *SePDC1$_p$-ARO2-SSA1t* shrDC *SeFBA1$_p$-ARO9-ADH1t* shrDD *SeGPM1$_p$-ARO7^{T226I}-TEF1t* shrDE *ENO2$_p$-ARO1 sga1Δ::ENO2$_p$-TKL1-TDH3t* pGGKd019 (*CEN6/ARS4, URA3*)	This study
IMX2068	*ura3-52 can1Δ::Spcas9-natNT2 tyr1$_p$Δ::YEN1$_p$-TYR1*	This study
IMX2069	*ura3-52 can1Δ::Spcas9-natNT2 tyr1$_p$Δ::AGE1$_p$-TYR1*	This study
IMX2071	*ura3-52 can1Δ::Spcas9-natNT2 tyr1$_p$Δ::SEC18$_p$-TYR1*	This study
IMX2072	*ura3-52 can1Δ::Spcas9-natNT2 tyr1$_p$Δ::MRI$_p$-TYR1*	This study
IMX2073	*ura3-52 can1Δ::Spcas9-natNT2 aro3Δ TDH3$_p$-ARO4^{K229L}-ENO2t* shrDA *SkTDH3$_p$-PHA2-TEF2t* shrDB *SePDC1$_p$-ARO2-SSA1t* shrDC *SeFBA1$_p$-ARO9-ADH1t* shrDD *SeGPM1$_p$-ARO7^{T226I}-TEF1t* shrDE *ENO2$_p$-ARO1 sga1Δ::ENO2$_p$-TKL1-TDH3t tyr1$_p$::YEN1$_p$-TYR1*	This study
IMX2074	*ura3-52 can1Δ::Spcas9-natNT2 aro3Δ TDH3$_p$-ARO4^{K229L}-ENO2t* shrDA *SkTDH3$_p$-PHA2-TEF2t* shrDB *SePDC1$_p$-ARO2-SSA1t* shrDC *SeFBA1$_p$-ARO9-ADH1t* shrDD *SeGPM1$_p$-ARO7^{T226I}-TEF1t* shrDE *ENO2$_p$-ARO1 sga1Δ::ENO2$_p$-TKL1-TDH3t tyr1$_p$Δ::AGE1$_p$-TYR1*	This study
IMX2076	*ura3-52 can1Δ::Spcas9-natNT2 aro3Δ TDH3$_p$-ARO4^{K229L}-ENO2t* shrDA *SkTDH3$_p$-PHA2-TEF2t* shrDB *SePDC1$_p$-ARO2-SSA1t* shrDC *SeFBA1$_p$-ARO9-ADH1t* shrDD *SeGPM1$_p$-ARO7^{T226I}-TEF1t* shrDE *ENO2$_p$-ARO1 sga1Δ::ENO2$_p$-TKL1-TDH3t tyr1$_p$Δ::SEC18$_p$-TYR1*	This study
IMX2077	*ura3-52 can1Δ::Spcas9-natNT2 aro3Δ ARO1$_p$::TDH3$_p$-ARO4^{K229L}-ENO2t* shrDA *SkTDH3$_p$-PHA2-TEF2t* shrDB *SePDC1$_p$-ARO2-SSA1t* shrDC *SeFBA1$_p$-ARO9-ADH1t* shrDD *SeGPM1$_p$-ARO7^{T226I}-TEF1t* shrDE *ENO2$_p$-ARO1 sga1Δ::ENO2$_p$-TKL1-TDH3t tyr1$_p$Δ::MRI$_p$-TYR1*	This study
IMX2102	*ura3-52 can1Δ::Spcas9-natNT2 aro3Δ aro8Δ TDH3$_p$-ARO4^{K229L}-ENO2t* shrDA *SkTDH3$_p$-PHA2-TEF2t* shrDB *SePDC1$_p$-ARO2-SSA1t* shrDC *SeFBA1$_p$-ARO9-ADH1t* shrDD *SeGPM1$_p$-ARO7^{T226I}-TEF1t* shrDE *ENO2$_p$-ARO1 sga1Δ::ENO2$_p$-TKL1-TDH3t PYK1^{A336S} pUDR574 (KlURA3,* gRNA-*PYK1.2)*	This study
IMX2106	*ura3-52 can1Δ::Spcas9-natNT2 aro3Δ aro8Δ TDH3$_p$-ARO4^{K229L}-ENO2t* shrDA *SkTDH3$_p$-PHA2-TEF2t* shrDB *SePDC1$_p$-ARO2-SSA1t* shrDC *SeFBA1$_p$-ARO9-ADH1t* shrDD *SeGPM1$_p$-ARO7^{T226I}-TEF1t* shrDE *ENO2$_p$-ARO1 sga1Δ::ENO2$_p$-TKL1-TDH3t PYK1^{DA336S}*	This study

(*continued on next page*)

Table 1 (*continued*)

Strain	Relevant genotype	Reference
IMX2107	*ura3-52 can1Δ::Spcas9-natNT2 aro3Δ aro8Δ ARO1$_p$::TDH3$_p$-ARO4^{K229L}-ENO2t* shrDA *SkTDH3$_p$-PHA2-TEF2t* shrDB *SePDC1$_p$-ARO2-SSA1t* shrDC *SeFBA1$_p$-ARO9-ADH1t* shrDD *SeGPM1$_p$-ARO7^{T226I}-TEF1t* shrDE *ENO2$_p$-ARO1 sga1Δ::ENO2$_p$-TKL1-TDH3t PYK1^{D146N} pUDR577 (KlURA3,* gRNA-*PYK1.1)*	This study
IMX2108	*ura3-52 can1Δ::Spcas9-natNT2 aro3Δ aro8Δ TDH3$_p$-ARO4^{K229L}-ENO2t* shrDA *SkTDH3$_p$-PHA2-TEF2t* shrDB *SePDC1$_p$-ARO2-SSA1t* shrDC *SeFBA1$_p$-ARO9-ADH1t* shrDD *SeGPM1$_p$-ARO7^{T226I}-TEF1t* shrDE *ENO2$_p$-ARO1 sga1Δ::ENO2$_p$-TKL1-TDH3t PYK1^{D146N}*	This study
IMX2123	*ura3-52 can1Δ::Spcas9-natNT2 aro3Δ aro8Δ TDH3$_p$-ARO4^{K229L}-ENO2t* shrDA *SkTDH3$_p$-PHA2-TEF2t* shrDB *SePDC1$_p$-ARO2-SSA1t* shrDC *SeFBA1$_p$-ARO9-ADH1t* shrDD *SeGPM1$_p$-ARO7^{T226I}-TEF1t* shrDE *ENO2$_p$-ARO1 sga1Δ::ENO2$_p$-TKL1-TDH3t tyr1$_p$Δ::YEN1$_p$-TYR1 PYK1^{DA336S}*	This study
IMX2124	*ura3-52 can1Δ::Spcas9-natNT2 aro3Δ aro8Δ TDH3$_p$-ARO4^{K229L}-ENO2t* shrDA *SkTDH3$_p$-PHA2-TEF2t* shrDB *SePDC1$_p$-ARO2-SSA1t* shrDC *SeFBA1$_p$-ARO9-ADH1t* shrDD *SeGPM1$_p$-ARO7^{T226I}-TEF1t* shrDE *ENO2$_p$-ARO1 sga1Δ::ENO2$_p$-TKL1-TDH3t tyr1$_p$Δ::YEN1$_p$-TYR1 PYK1^{D146N}*	This study
IME471	*ura3-52 can1Δ::Spcas9-natNT2 aro3Δ aro8Δ TDH3$_p$-ARO4^{K229L}-ENO2t* shrDA *SkTDH3$_p$-PHA2-TEF2t* shrDB *SePDC1$_p$-ARO2-SSA1t* shrDC *SeFBA1$_p$-ARO9-ADH1t* shrDD *SeGPM1$_p$-ARO7^{T226I}-TEF1t* shrDE *ENO2$_p$-ARO1 sga1Δ::ENO2$_p$-TKL1-TDH3t tyr1$_p$Δ::YEN1$_p$-TYR1 PYK1^{D146N}* pUDE001 *(2 µm URA3, TDH3$_p$-ARO10-CYC1t)*	This study
IMX2179	*ura3-52 can1Δ::Spcas9-natNT2 aro3Δ aro8Δ TDH3$_p$-ARO4^{K229L}-ENO2t* shrDA *SkTDH3$_p$-PHA2-TEF2t* shrDB *SePDC1$_p$-ARO2-SSA1t* shrDC *SeFBA1$_p$-ARO9-ADH1t* shrDD *SeGPM1$_p$-ARO7^{T226I}-TEF1t* shrDE *ENO2$_p$-ARO1 sga1Δ::ENO2$_p$-TKL1-TDH3t tyr1$_p$::YEN1$_p$-TYR1 X3::FBA1$_p$-ARO3^{K222L}-PGKIt* shrAF *PDC1$_p$-EcaroL-ADH3t PYK1^{D146N}* pUDE001 *(2 µm URA3, TDH3$_p$-ARO10-CYC1t)*	This study
IMX2222	*ura3-52 can1Δ::Spcas9-natNT2 aro3Δ aro8Δ TDH3$_p$-ARO4^{K229L}-ENO2t* shrDA *SkTDH3$_p$-PHA2-TEF2t* shrDB *SePDC1$_p$-ARO2-SSA1t* shrDC *SeFBA1$_p$-ARO9-ADH1t* shrDD *SeGPM1$_p$-ARO7^{T226I}-TEF1t* shrDE *ENO2$_p$-ARO1 sga1Δ::ENO2$_p$-TKL1-TDH3t tyr1$_p$Δ::YEN1$_p$-TYR1 X3::FBA1$_p$-ARO3^{K222L}-PGKIt* shrAF *PDC1$_p$-EcaroL-ADH3t gpp1Δ::PGK1p-Bbxfpk-ENO1t shrBA PGI1p -Ckpta-TDH1t PYK1^{D146N}* pUDE001 *(2 µm URA3, TDH3$_p$-ARO10-CYC1t)*	This study
IMX2279	*ura3-52 can1Δ::Spcas9-natNT2 aro3Δ aro8Δ TDH3$_p$-ARO4^{K229L}-ENO2t* shrDA *SkTDH3$_p$-PHA2-TEF2t* shrDB *SePDC1$_p$-ARO2-SSA1t* shrDC *SeFBA1$_p$-ARO9-ADH1t* shrDD *SeGPM1$_p$-ARO7^{T226I}-TEF1t* shrDE *ENO2$_p$-ARO1 sga1Δ::ENO2$_p$-TKL1-TDH3t tyr1$_p$Δ::YEN1$_p$Δ-TYR1 X3::FBA1$_p$-ARO3^{K222L}-PGKIt* shrAF *PDC1$_p$-EcaroL-ADH3t X2::PYK1$_p$-ADH2-PDC1t PYK1^{D146N}* pUDE001 *(2 µm URA3, TDH3$_p$-ARO10-CYC1t)*	This study

PFK2$_t$, *FBA1$_t$*, *TDH3$_t$*, *GPM1$_t$*, *PDC1$_t$* and *ADH3$_t$* regions were synthesized (GeneArt, ThermoFisher Scientific). In this case, the terminators were flanked upstream with the terminator specific YeastToolkit flank ' AAGCATCGTCTCATCGGTCTCAATCC' and downstream with 'TTATGC CGTCTCAGGTCTCACAGC' (Lee et al., 2015). All terminator fragments were assembled into entry vector pUD565 resulting in part plasmids pGGKp037 (*ADH1$_t$*), pGGKp038 (*TEF2$_t$*), pGGKp039 (*TEF1t*), pGGKp040 (*PYK1$_t$*), pGGKp041 (*TDH3$_t$*), pGGKp045 (*PDC1$_t$*), pGGKp048 (*GPM1$_t$*), pGGKp099 (*PGI1$_t$*), pGGKp101 (*PFK1$_t$*), pGGKp103 (*PFK2$_t$*), pGGKp105 (*FBA1$_t$*), pGGKp106 (*TDH3$_t$*) pGGKp107 (*GPM1$_t$*), pGGKp110 (*PDC1$_t$*) and pGGKp113 (*ADH3$_t$*).

The ORFs were also obtained from genomic DNA of CEN.PK113-7D using primers with gene part type specific overhangs (TATG and GGAT) (Table S1). Primer pairs 16497/16498, 11580/11581 and 13106/13107 were used to obtain fragments *ADH2, TKL1* and *PHA2.* Because the ORF of *TYR1, ARO9, ARO8* and *ARO2* contained internal BsaI and/or BsmbI sites, these restriction sites were removed from the coding sequence by amplifying the gene in multiple fragments using overlap primers that introduced silent mutations, thereby removing the internal restriction site and adding an additional BsmBI site, which would be lost after BsmBI assembly. For the 5′ end of the reverse primer the overlap 5′-CACGTCTCANNNN(primer sequence)-3′ was used where NNNN is the 4-base stretch for replacing the internal site. For the forward primer the overlap 5′-TTCGTCTCTNNNN(primer sequence)-3′ was used, again using the NNNN stretch for removing the same site. Since *ARO2* contained one BsmBI site close to the start of the gene, only the BsaI site was removed from this gene. The *TYR1* ORF was amplified using primer pairs 13111/13109 and 13108/13110, *ARO9* with 13104/13103 and 13102/13105, *ARO8* with 13100/13099 and 13098/13101 and *ARO2* with 13096/13093 and 13092/13097. The Bbxfpk ORF was amplified from plasmid pAB3 (Table S1) using primers 15374 and 15375. The *ARO7^{T226I}*, *ARO3^{K222L}*, *ARO4^{K229L}*, *EcaroG^{P150L}*, *EcaroB, EcaroD, EcaroE, EcaroL, EcaroA, EcaroC*, *EcpheA^{T326P}* and *Ckpta genes* were synthesized using the Invitrogen GeneArt gene synthesis service (ThermoFisher Scientific). The sequences for the *E. coli* genes were derived from the annotated genome of strain K-12 substr. MG1655 (Bioproject accession number PRJNA225; assembly GCA_000005845.2) and the sequence from *Ckpta* was derived from *Clostridium kluyveri* strain ATCC8527 (Bioproject accession number A5N801). All genes were ordered codon optimised. Any internal BsmBI/BsaI sites were removed from the sequence using silent mutations and the ORFs were flanked upstream with the gene specific YeastToolkit flank 'AAGCATC GTCTCATCGGTCTCAT' and downstream with 'TTATGCCGTCTCAGGT CTCAGGAT'. The amplified and synthesized fragments were cloned into entry vector pUD565, via BsmBI Golden Gate assembly, resulting in part plasmids pGGKp118 (*ARO7^{T226I}*), pGGKp119 (*EcaroG^{P150L}*), pGGKp120 (*EcaroB*), pGGKp121 (*EcaroD*), pGGKp122 (*EcaroE*), pGGKp123 (*EcaroL*), pGGKp124 (*EcaroA*), pGGKp125 (*EcaroC*), pGGKp126 (*EcpheA^{T326PL}*), pGGKp134 (*ARO4^{K229L}*), pGGKp165 (*ARO8*), pGGKp166 (*ARO9*), pGGKp167 (*PHA2*), pGGKp168 (*TYR1*), pGGKp170 (*ARO2*), pGGKp246 (*ARO3^{K222L}*), pGGKp236 (*Ckpta*), pGGKp240 (*Bbxfpk*) and pGGKp294 (*ADH2*). The amplified *TKL1* fragment was assembled into entry vector pUD564 resulting in part plasmid pGGKp067 (*TKL1*).

Correct construction of part plasmids would result in the replacement of the GFP gene by the target gene which allows visual screening of the colonies. Additional plasmid confirmation was done by colony PCR using primers 2012 and 2397. Correct removal of internal BsaI/BsmBI sites of *ARO2, TYR1, ARO8* and *ARO9* was verified by Sanger sequencing (BaseClear, leiden, NL).

To construct the expression cassettes to engineer 2PE production in *S. cerevisiae*, first recipient GFP dropout plasmids were constructed by BsmBI Golden Gate assembly using the yeast tool kit principle outlined by Lee et al. (2015). The first one, PGGKd005 was obtained by assembling the part plasmids pYTK002 and pYTK067 (left and right connectors), pYTK047 (GFP dropout), pYTK079 (*hghR*), pYTK081 (*CEN6/ARS4* yeast replication origin) with pYTK083 (bacterial origin of replication factor and ampicillin resistance (*bla*) gene). pGGKd015 was constructed by golden gate assembly of pYTK002 and pYTK067 (left and right connectors respectively), pYTK047 (GFP dropout) and pYTK095 (bacterial origin of replication factor and ampicillin resistance gene). pGGKd019 was constructed by combining pYTK002 and pYTK073 (left and right connectors), pYTK047 (GFP dropout), pYTK074 (*URA3*), pYTK081 (*CEN6/ARS4* yeast replication origin) with

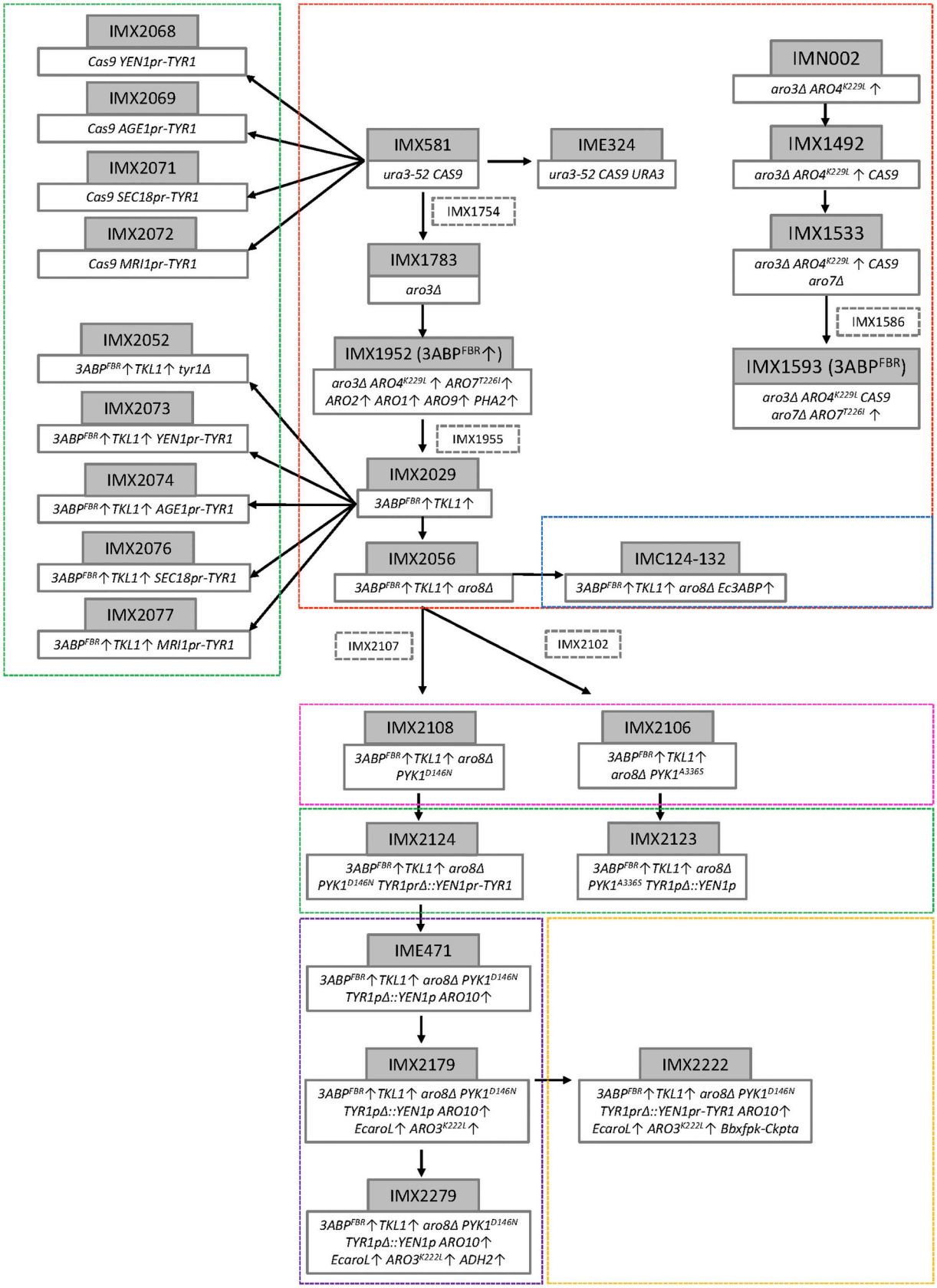

Fig. 2. Strain genealogy of constructed strains in this study. The strain name is depicted in a grey box and the relevant genotype is depicted in a box with grey outlines. Strain names in a white box with a dashed line are intermediate strains still carrying a plasmid expressing *cas9* gRNA. The strains are grouped according to their main metabolic engineering strategy. Established approached (red), *TYR1* downregulation (green), *E. coli* complementation (blue), increasing PEP supply (pink), overexpression of the Ehrlich pathway (purple) and increasing E4P supply (yellow). (For interpretation of the references to colour in this figure legend, the reader is referred to the Web version of this article.)

pYTK084 (bacterial origin of replication factor and kanamycin resistance gene). Finally, pGGKd046 was assembled using part plasmids pYTK003 and pYTK072 (left and right connectors), pYTK047 (GFP dropout), pYTK078 (*natR*), pYTK081 (*CEN6/ARS4* yeast replication origin) with pYTK083 (bacterial origin of replication factor and ampicillin resistance gene).

Next, a specific promoter, gene and terminator part plasmid were assembled into one of the GFP dropout plasmids via BsaI mediated Golden Gate assembly resulting in expression cassettes. As example, pGGKp028 ($ENO2_p$), pGGKp041 ($TDH3_t$) and pGGKp067 (*TKL1*) were assembled into pGGKd015 resulting in pUD660 ($ENO2_p$-*TKL1*-$TDH3_t$). A full overview of the constructed expression cassettes and the part plasmids used for the construction is given in Table S2. Colony PCR for initial screening was performed on randomly picked colonies using primers 10320 and 10327 for expression cassettes with the pGGKd005 or pGGKd015 backbone and primers 10320 and 10335 for the pGGKd019 or pGGkd046 backbone. Final plasmid confirmation was done by restriction analysis.

2.4. Strain construction

Integration of *Spcas9* into IMN002 was performed by assembling and integrating the *Spycas9* and natNT2 marker cassettes into the *SPR3* locus. The integration cassette containing the *cas9* gene was amplified using p414-$TEF1_p$-*cas9*-$CYC1_t$ (DiCarlo et al., 2013) as DNA template with primers 12036 and 4653, adding homologous flanks for integration into the *SPR3* locus and a short homologous sequence (shr) (Kuijpers et al., 2013) facilitating homologous recombination. The natNT2 integration cassette was amplified using primer pair 3093 and 12037 with pUG-natNT2 (de Kok et al., 2011) as template using an initial denaturation of 1 min instead of the advised 30 s and 20 s denaturation instead of 10 s. The constructed strain was stocked as IMX1492. Correspondingly, IMX1492 was co-transformed with the linearized backbone of pMEL10 (Mans et al., 2015, 2018), the double-stranded cassette (primers 12048 & 12049) containing the gRNA for *ARO7* together with the double stranded repair oligo (primers 12050 & 12051) for knocking out *ARO7*. The resulting *aro7Δ* strain was stocked as IMX1533 after plasmid recycling. Next, the $ARO7^{T226I}$ cassette was PCR amplified from pUD714 using primers 12248 and 12249, adding flanks for integration in the *ARO7* promoter region. IMX1533 was transformed with the purified PCR product, pUDR649 (gRNA-$ARO7_p$) leading to strain IMX1586 and IMX1593 ($3ABP^{FBR}$) before and after plasmid recycling, respectively.

IMX581 was transformed with pGGKd019 (*CEN6/ARS4, URA3*) resulting in IME324. Additionally, IMX581 was transformed with pUDR409 (gRNA-*ARO3*) and the double-stranded repair oligo (primer 13594 & 13595) for deleting *ARO3,* resulting in strain IMX1754 and IMX1783 before and after plasmid recycling.

Next, the integration cassettes for all 3ABP genes except *ARO1* were obtained by PCR amplification using primers adding homologous flanks for integration into the *ARO1* promoter region or shr flanks facilitating *in vivo* assembly of the cassettes. Since *ARO1* is a large gene of 4767 bp, its overexpression was achieved by replacing the native promoter by the strong consecutive promoter $ENO2_p$. Primers 14173 & 14174 were used to amplify the $ARO4^{K229L}$ fragment using pUD759 as template DNA. The *PHA2* cassette was amplified using primers 12656 & 12666 and pUD754 as template DNA. Primers 14175 & 14176 were used to amplify the *ARO2* region using pUD760. pUD804 was used as template to amplify the *ARO9* fragment with primers 14177 & 14463. Primer pair 14302 & 14459 were used to obtain the $ARO7^{T226I}$ region with pUD714 as template. Finally, the *ENO2* promoter was amplified from pGGKp028 using primers 12660 & 14181. All obtained fragments were co-transformed in IMX1783 together with pUDR478 (gRNA-$ARO1_p$), targeting the *ARO1* promoter. Subsequently, pUDR478 was recycled and the strain containing overexpressed (feedback resistant) alleles of all 3ABP genes without plasmid was stocked as IMX1952 ($3ABP^{FBR}$↑).

Integration of the overexpression cassette for *TKL1* was done by amplifying the region with primers 12047 and 14563 from pUD660 adding 60 bp homology flanks to *SGA1*. The obtained fragment was co-transformed together pUDR372 (gRNA-*SGA1*) resulting in strain IMX1955 and IMX2029 before and after plasmid removal, respectively. Subsequently, *ARO8* was deleted in IMX2029 by transforming this strain with pUDR553 (gRNA-*ARO8)* and an *ARO8* repair oligo (primers 8856 & 8857). pUDR553 was then recycled and the strain was stocked as IMX2056. IMX2056 was then transformed with pUDC245-pUDC252 or pGGKd015 resulting in strains IMC124 ($EcaroG^{P150L}$), IMC125 (*EcaroB*), IMC126 (*EcaroD*), IMC127 (*EcaroE*), IMC128 (*EcaroL*), IMC129 (*EcaroA*), IMC130 (*EcaroC*), IMC131 ($EcpheA^{T326PL}$) and IMC132 (*URA3*).

The native *TYR1* promoter of IMX2029 was replaced by four different promoters ($AGE1_p$, $MRI1_p$, $SEC18_p$, and $YEN1_p$). Primer pairs 14948 & 14947, 14998 & 14952, 14999 & 14949 and 14945 & 14946 were used to amplify the $AGE1_p$, $MRI1_p$, $SEC18_p$ and $YEN1_p$ regions, respectively. Obtained promoter regions contained 60 bp homology flanks to the *TYR1* promoter region and *TYR1*. The exact promoter sequence of $YEN1_p$ was already described and shown to lead to low gene expression (Papapetridis et al., 2018). For $AGE1_p$, 800 nucleotides upstream of the gene were used as promoter region. For the $MRI1_p$ and $SEC18_p$ all the nucleotides until the upstream gene were used as promoter region. By Cas9 mediated editing using pUDR568 (gRNA-$TYR1_p$) and the individual promoter integration fragments, the native *TYR1* promoter was replaced by one of the four promoters in both the IMX581 and the IMX2029 background. After plasmid removal, for the IMX581 background this resulted in strains IMX2068 ($YEN1_p$-*TYR1*), IMX2069 ($AGE1_p$-*TYR1*), IMX2071 ($SEC18_p$-*TYR1*) and IMX2072 ($MRI1_p$-*TYR1*). From IMX2029 background, the strains IMX2073 ($YEN1_p$-*TYR1*), IMX2074 ($AGE1_p$-*TYR1*), IMX2076 ($SEC18_p$-*TYR1*) and IMX2077 ($MRI1_p$-*TYR1*) were constructed after discarding its plasmids. In order to study the effect of a complete *TYR1* knockout, IMX581 and IMX2029 were also transformed with pUDR550 (gRNA-*TYR1*) and a repair oligo consisting of an artificial gRNA (primers 14935 & 14936) resulting in strains IMX2051 and IMX2052, respectively, after plasmid removal.

IMX2056 was transformed with pUDR574 (gRNA-*PYK1.1*) using repair oligo 14853 & 14854 or with pUDR577 (gRNA-*PYK1.2*) using repair oligo 14851 & 14852, to obtain silent mutations in *PYK1*. The SNPs were confirmed using Sanger sequencing and stored as IMX2102 ($PYK1^{A336S}$) and IMX2107 ($PYK1^{D147N}$), respectively and as IMX2106 ($PYK1^{A336S}$) and IMX2108 ($PYK1^{D147N}$) after losing their plasmid.

In both IMX2106 and IMX2108, the native $TYR1_p$ promoter was replaced using the same cas9 plasmid (pUDR568) and the same $YEN1_p$ integration fragment as described before resulting in strains IMX2123 and IMX2124, respectively after discarding the plasmid. Next, IME471 was obtained by transforming IMX2124 with the episomal plasmid pUDE001 overexpressing *ARO10* (Vuralhan et al., 2005).

Subsequently, IME471 was transformed with *EcaroL* and $ARO3^{K222L}$ integration cassettes using pUDR599 (gRNA-*X3*) for the cas9 targeting of the *X3* region (Strucko et al., 2017). pUDC249 served as template for amplifying *EcaroL,* whereas $ARO3^{K222L}$ was obtained from pUD1037. *EcaroL* and $ARO3^{K222L}$ integration cassettes were amplified using primers 15831 & 15697 and 15694 & 15830, respectively, obtaining strain IMX2179 (*Ec.aroL*↑ $ARO3^{K222L}$↑) after plasmid removal.

Next, the *Bbxfpk* expression cassette was amplified from pUDC289 using primer pair 15377 & 16009 and the *Ckpta* expression cassette was obtained using primers 15333 & 16008 with pUDC290 as template (Bergman et al., 2016). Both fragments were cotransformed in IMX2179 together with pUDR598 (gRNA-*GPP1*) for targeting *GPP1* resulting in strain IMX2222 after discarding the plasmid.

Finally, the *ADH2* ORF was amplified from pUD1091 using primers 12934 and 16499, adding flanks with homology to the *X2* intergenic region. IMX2179 was transformed with the obtained fragment and pUDR547 (gRNA-*X2*) targeting the X2 region. After recycling the plasmid the strain was stocked as IMX2279 (*ADH2*↑). An overview of

the strain genealogy is given in Fig. 2.

All transformed strains were re-streaked three times prior to stocking. Correct integration or deletion was checked using colony PCR using diagnostic primers given in Table S1. When required, plasmid removal in all strains was performed by growing the strain without the selective pressure required for retaining the plasmid. After obtaining single colonies, a single colony was re-streaked on both selective and non-selective medium. The colony growing only on non-selective medium was assumed to have discarded its plasmid and was used to inoculate liquid medium and stocked (Mans et al., 2018; Wijsman et al., 2019).

2.5. Characterization of tyrosine prototrophy

To study potential growth defects caused by tyrosine auxotrophy of the *TYR1* promoter replacement strains, spot plate assays were performed. The number of cells of exponentially growing strain cultures were counted using the Z2 Coulter counter (Beckman Coulter, Indianapolis, IN) according to manufacturer's protocol. The cultures were washed and dilutions of 10^6, 10^5, 10^4 and 10^3 cells per 0.5 mL were prepared using sterile demineralized H_2O. Of each of these dilutions, 5 µL was spot-plated on petri plates containing YPD, SMG (Ura) and SMG (Ura + Tyr). Plates were incubated at 30 °C for 48 h (YPD) to 72 h (SMG).

2.6. Strain characterization

Growth rates were obtained from aerobic batch cultures grown in independent biological duplicates. Exponentially growing cells from the same medium and temperature were used to inoculate 500 mL shake flasks containing 100 mL SMG with additional uracil when required at a starting OD_{660} of 0.5.

For 2PE production studies, all strains were inoculated at a starting OD_{660} of 0.2 in biological triplicates. The cells were grown for 24 or 48 h based on the time required to deplete all glucose. Samples were centrifuged for 5 min at 16,050 g and the supernatant was collected for metabolite analysis.

Extracellular organic acids, sugars and ethanol were determined by high performance liquid chromatography (HPLC) analysis using an Aminex HPX-87H ion-exchange column (Agilent, Santa Clara, CA) with 5 mM H_2SO_4 as mobile phase and a flow rate of 0.6 mL min^{-1} at 60 °C. Glucose, glycerol, and ethanol were detected by a refractive-index detector (Agilent G1362A) and organic acids by a dual-wavelength absorbance detector (Agilent G1314F). Ehrlich metabolites (2PE, *p*OH2PE, PPA, PPY, CHR, SHK, *p*OHPPY, *p*OHPAA were measured using an Agilent Zorbax Eclipse plus C18 column (4.6 x 100 mm, 3.5 µm) (Agilent) with 0.020 M KH_2PO_4 (pH 2.0) and 1% acetonitrile as mobile phase with a flow rate of 0.8 mL min^{-1} at 40 °C. The amount of acetonitrile was increased to 10% in 6 min, followed by an increase to 40% until 23 min. From 23 to 27 min the amount of acetonitrile was reduced to 1% again and kept at this amount until 30 min. Detection of compounds occurred by means of a diode array and multiple wavelength detector (Agilent G1315C) at different wavelengths: 200 nm for *p*OH2PE, PPY, and PAA, 214 nm for shikimate and 2-phenylethanol, 280 nm for *p*OHPAA and 310 nm for *p*OHPPY.

Aerobic batch bioreactor cultures were performed in 2-L bioreactors (Applikon, Delft, The Netherlands) using a working volume of 1.2 L. The bioreactors were filled with synthetic medium with extra nitrogen source (SMN). SMN contained 3 g L^{-1} KH_2PO_4, 0.5 g L^{-1} $MgSO_4 \cdot 7H_2O$, and trace elements and 10 g L^{-1} $(NH_4)_2SO_4$ to avoid nitrogen limitation (Koopman et al., 2012). After heat sterilization of the bioreactors, 20 g L^{-1} glucose, 0.2 g L^{-1} antifoam C (Sigma-Aldrich, Zwijndrecht, The Netherlands), and filter-sterilized vitamins solution were added (Verduyn et al., 1992).

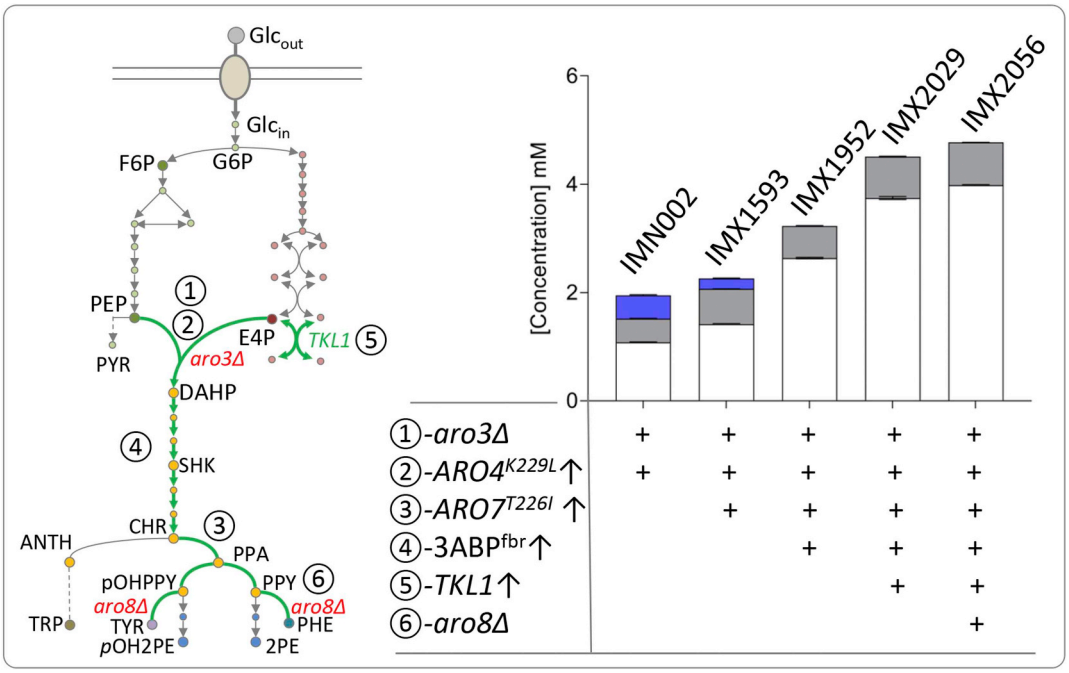

Fig. 3. Recapitulation of validated modifications affecting the aromatic amino acid biosynthesis pathway. Left panel-schematic representation of the genetic modifications introduced in strains IMN002 (Luttik et al., 2008), IMX1593, IMX1952, IMX2029 and IMX2056. The modifications include ① the *ARO3* deletion, ② alleviation of allosteric regulation of the DAHP synthase, ③ alleviation of allosteric regulation of the chorismate mutase, ④ overexpression of the aromatic amino acid biosynthetic pathway comprising feedback insensitive variants of Aro4 and Aro7, ⑤ overexpression of the transketolase Tkl1 and ⑥ the deletion of *ARO8*. The green arrows denote an overexpression. Right panel- Production of 2PE (white bar), *p*OH2PE (grey bar), shikimate (blue bar) in (mM). Strains were grown at 30 °C for 24 h at 200 RPM in 500 mL shake flasks containing 100 mL minimal synthetic medium supplemented with 150 mg L^{-1} uracil when required and 20 g L^{-1} glucose as carbon source. The values represent averages ± mean deviations of data obtained from independent triplicate cultures. + denotes the presence of a set of genetic modifications in a given strain. (For interpretation of the references to colour in this figure legend, the reader is referred to the Web version of this article.)

The bioreactors were inoculated from exponentially growing cells in preculture shake flasks containing 100 mL of SMG to an initial biomass concentration of 0.08 g L^{-1}. The aerobic batch cultivations were performed at 30 °C at a stirrer speed of 800 rpm. The culture pH was maintained at 5.0 by automated addition of 2 M KOH and pressurized air was sparged through the bioreactors at 0.6 L min^{-1} to supply oxygen and strip produced carbon dioxide.

Optical density was measured by using a Jenway 7200 spectrophotometer (Jenway, Staffordshire, United Kingdom) at 660 nm. Cell dry weights were determined via filtration of 10 mL of well-mixed sample over dry nitrocellulose membrane filters with a pore size of 0.45 µm (Pall Corporation, Port Washington, NY). Filters were washed with demineralized water and dried in a microwave oven for 20 min at 360 W.

For analysis of carbon dioxide production and oxygen consumption in the bioreactor, the off-gas was first cooled in a condenser on the bioreactor (2 °C) and dried with a Permapure MD-110-48P-4 dryer (Permapure, Lakewood, NJ), after which CO_2 and O_2 concentrations in the off-gas were measured with a NGA 2000 Rosemount gas analyser (Rosemount Analytical, Irvine, CA).

3. Results

3.1. Effects of the alleviation of allosteric regulation of the aromatic amino acid biosynthetic pathway, its overexpression and the supply of erythrose-4-P through transketolase are additive with respect to 2PE synthesis

The aromatic amino acid biosynthesis pathway has been intensively exploited to produce a wide range of metabolites that derive from the aromatic amino acid biosynthetic pathway such as stilbenoids e.g. resveratrol (Shen et al., 2016; Shin et al., 2011), hydroxycinnamic acids e.g. as *trans*-cinnamic acid (Gottardi et al., 2017a, 2017b) or *p*-coumaric acid (Rodriguez et al., 2017), flavonoids e.g. naringenin, kaempferol (Koopman et al., 2012; Rodriguez et al., 2017) or anthocyanin (Eichenberger et al., 2018; Levisson et al., 2018) and even opioids (Galanie et al., 2015). All these compounds share the yeast precursors phenylalanine and/or tyrosine. In contrast to the presented work, in these reference production strains the capacity to produce 2PE had to be reduced or eliminated since it represents an unwanted by-product. In a first step towards increasing 2PE production, we verified that some of the metabolic engineering strategies proposed for the biosynthesis of these phenylalanine and tyrosine derived compounds were also beneficial for *de novo* 2PE production.

The alleviation of the allosteric feedback regulation of the DAHP synthases and to a lesser extend of the chorismate mutase activities have been shown to be instrumental for *de novo* production of 2PE. The strains IMN002 (*aro3*Δ $ARO4^{K229L}$↑) (Luttik et al., 2008) and IMX1593 (*aro3*Δ $ARO4^{K229L}$↑ $ARO7^{T226I}$↑) produced more than 1mM extracellular aromatic higher alcohols, while the control strain IMX581 did not produce any. Both IMN002 and IMX1593 did produce detectable amounts of shikimate in the supernatant. Subsequently, the native *ARO1* promoter was exchanged by the strong consecutive enolase 2 gene *ENO2* promoter (Boonekamp et al., 2018) and the overexpression cassettes of $ARO4^{K229L}$, $ARO7^{T226I}$ and the remaining 3ABP genes *ARO2, ARO9* and *PHA2* were introduced upstream of the *ARO1* locus assembling a 3ABP genes cluster on CHRIV. The resulting strain IMX1952 produced 56% more aromatic higher alcohols. The increase was mainly attributed to 2PE that increased by 86%, while *p*OH2PE slightly decreased by 9% (Fig. 3).

Next, to maximize the flux towards erythrose-4-phosphate, the transketolase gene *TKL1* was overexpressed. In contrast to the previous work (Curran et al., 2013), this overexpression was not coupled with the deletion of the glucose-6-phosphate dehydrogenase gene *ZWF1* since *ZWF1* deletion resulted in an excessive reduction in growth rate. The strain IMX2029 (*aro3*Δ $ARO4^{K229L}$↑ $ARO7^{T226I}$↑ 3ABP↑ *TKL1*↑) secreted an extra 40% and 118% of aromatic higher alcohols relative to IMX1952 and IMX1593.

Finally, the deletion of *ARO8* that encodes an aromatic aminotransferase with broad substrate specificity was introduced in IMX2029. The 2PE and *p*OH2PE extracellular concentrations of IMX2056 (*aro3*Δ *aro8*Δ $ARO4^{K229L}$↑ $ARO7^{T226I}$↑ 3ABP↑ *TKL1*↑) cultures were only 6% higher than that of the parental strain IMX2029 reaching 3.81 ± 0.03 mM and 0.75 ± 0.02 mM, respectively, after 24 h of shake flask cultivations, still representing a small but significant increase (Table S3).

3.2. Overexpression of EcaroL (shikimate kinase) eliminates the formation of shikimate and improves 2PE biosynthesis

The first strains of the lineage IMN002 (*aro3*Δ $ARO4^{K229L}$↑) and IMX1593 (*aro3*Δ $ARO4^{K229L}$↑ $ARO7^{T226I}$↑) were excreting low but measurable shikimate quantities, suggesting a catalytic limitation downstream the shikimate point. In *S. cerevisiae*, the main part of the shikimate pathway is catalysed by a pentafunctional enzyme Aro1, which complicates tuning gene expression at individual activity level. In *E. coli*, the shikimate pathway reactions are catalysed by enzymes encoded by individual genes. To systematically evaluate the impact of each single *E. coli* gene, the strain IMX2056 (*aro3*Δ *aro8*Δ $ARO4^{K229L}$↑ $ARO7^{T226I}$↑ 3ABP↑ *TKL1*↑) was transformed with plasmids expressing a single (feedback resistant) *E. coli* gene ($EcaroG^{P150L}$, *EcaroB, EcaroD, EcaroE, EcaroL, EcaroA, EcaroC* and $EcpheA^{T326P}$). The strains IMC124 to IMC131 were compared to the reference strain IMC132, which corresponds to IMX2056 transformed with an empty *URA3* plasmid to restore strain prototrophy. Independent of whether the overexpressed genes were located upstream or downstream of shikimate in the pathway, the corresponding strains were still producing shikimate with strain IMC128 (*EcaroL*) producing the lowest amount. Most interestingly, this was accompanied by a 29% increase of the $\Sigma_{(2PE+2pOH2PE)}$ (Fig. 4). These results were in line with previously published results (Rodriguez et al., 2015) that demonstrated that indeed the phosphorylation step of shikimate to shikimate 3-phosphate catalysed by

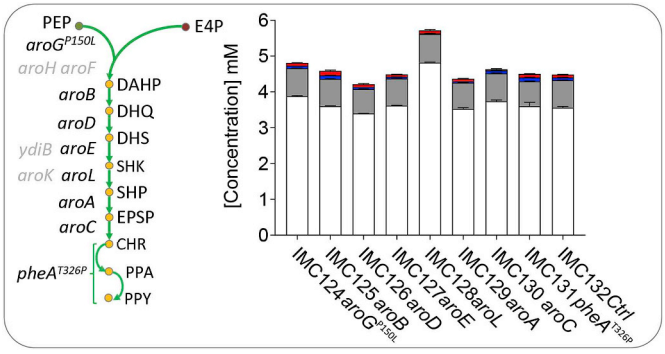

Fig. 4. Effect of the overexpression of single gene from the *E. coli* shikimate pathway *aroA-E*, $G^{P150(}$(that encodes a tyrosine insensitive DAHP synthase), *aroL* and $pheA^{T326P}$(that encodes a phenylalanine insensitive bi-functional chorismate mutase-prephenate dehydratase) on 2PE and *p*OH2PE biosynthesis in *S. cerevisiae*. Left panel-schematic representation of the *E. coli* shikimate pathway. The genes indicated in grey were not overexpressed. DAHP 3-deoxy-D-arabino-heptulosonate-7-phosphate, DHQ 3-dehydroquinate, DHS 3-dehydro-shikimate, SHK shikimate, SHP shikimate-3-phosphate, ESPS 5-enolpyruvyl-shikimate-3-phosphate, CHR chorismate and PPA prephenate. Right panel- Production of 2PE (white bar), *p*OH2PE (grey bar), SHK (blue bar) and phenylpyruvate (red bar) in (mM). Strains were grown at 30 °C for 24 h at 200 RPM in 500 mL shake flasks containing 100 mL minimal synthetic medium supplemented with 150 mg L^{-1} uracil when required and 20 g L^{-1} glucose as carbon source. The values represent averages ± mean deviations of data obtained from independent triplicate cultures. + denotes the presence of a set of genetic modifications in a given strain. (For interpretation of the references to colour in this figure legend, the reader is referred to the Web version of this article.)

shikimate kinase represented a target in metabolic engineering for the production of shikimate derived metabolites in *S. cerevisiae*.

3.3. Elimination of p-hydroxyphenylethanol (pOH2PE) biosynthesis leads to an increase of 2PE formation

In the engineered strains IMX1593, IMX1952, IMX2029 and IMX2056, extracellular *p*-hydroxyphenylethanol (*p*OH2PE) concentrations were ranging from 15 to 30% of the total aromatic higher alcohol produced. The latest common intermediate of the phenylalanine and tyrosine branches, prephenate, can be either directed to phenylalanine in a reaction catalysed by Pha2 that performs the dehydration of prephenate to phenylpyruvate or is directed to tyrosine in a reaction catalysed by Tyr1 that performs the oxidative decarboxylation of prephenate (PPA) yielding *p*-hydroxyphenylpyruvate (*p*OHPPY). The deletion of *TYR1* would eliminate the production of *p*OH2PE, but also introduce an auxotrophy for tyrosine, which is a rather undesirable trait. Instead, fine-tuning the expression of *TYR1* could lower the production of the by-product while preventing tyrosine auxotrophy. For this purpose, the suitable replacement for the *TYR1* promoter should be weaker, but also constitutively expressed to enable growth irrespective of the culture conditions. A microarray compendium of 170 steady-state chemostat cultures of the yeast *Saccharomyces cerevisiae* that encompass 55 unique conditions was investigated (Knijnenburg et al., 2007, 2009). In this compendium *TYR1* already exhibited a rather low expression (75.9 ± 23.4 AU) that is lower than average gene expression levels set at 110 in the compendium (Piper et al., 2002). In addition to a lower expression than *TYR1*, the selected genes should exhibit a coefficient of variation of its expression level lower than 25% over the entire conditions set. Four genes with expression profiles fulfilling these requirements were identified in the compendium (Table 2). The promoter sequences of *YEN1*, *AGE1*, *SEC18* and *MRI1* (832, 800, 362 and 257 bp, respectively) were cloned and used to replace the chromosomal *TYR1* promoter in the control strain IMX581. A deletion of *TYR1* in the same strain (IMX2051) cancelled growth on medium lacking tyrosine, an auxotrophy that can be rescued by addition of tyrosine in the culture medium or growth on complex medium (YPD). Meanwhile, the four constructed strains IMX2068 ($YEN1_p$), IMX2069 ($AGE1_p$), IMX071 ($SEC18_p$) and IMX2072 ($MRI1_p$) exhibited growth on chemically defined medium lacking tyrosine demonstrating the functionality of the four promoters. The three strains IMX2069 ($AGE1_p$), IMX071 ($SEC18_p$) and IMX2072 ($MRI1_p$) could grow as fast as the control strain IMX581 in tyrosine free medium (Table S3). In contrast, IMX2068 ($YEN1_p$) was significantly slower than IMX581 and the other three strains with a specific maximum growth rate (μ) of 0.33 ± 0.01 h^{-1} instead of 0.38 ± 0.00 h^{-1}.

Next, to evaluate the impact on the Ehrlich higher alcohol production, the *TYR1* promoter of strain IMX2029 (*aro3*Δ $ARO4^{K229L}$↑ $ARO7^{T226I}$↑ 3ABP↑ *TKL1*↑) was replaced by one of the four selected regulatory sequences. In this genetic background, a *TYR1* deletion was also sufficient to prevent growth on medium lacking tyrosine, an auxotrophy that can be rescued by addition of tyrosine in the culture medium or growth on complex medium (YPD) (Fig. 5). In contrast to the *tyr1Δ* mutant (IMX2052), all strains carrying the exchanged promoter were able the grow on medium without tyrosine (Fig. 5). The strains IMX2073 ($YEN1_p$), IMX2074 ($AGE1_p$), IMX2076 ($SEC18_p$) and IMX2077 ($MRI1_p$) were also grown for 24 h in chemically defined medium (SMG) and extracellular concentration of the Ehrlich metabolites were measured. Out of the four constructs only IMX2073 ($YEN1_p$) displayed a 90% reduced *p*OH2PE formation. Despite a slower growth rate the strain could still consume all sugars in 24 h and produce up to 6 mM of 2PE, which represents a significant 60% increase relative to the parental strain IMX2029 (Fig. 5). The *TYR1* promoter replacement by $YEN1_p$ has not only contributed to a near complete conversion of *p*OH2PE into 2PE but has also enabled a further increase of 2PE concentrations ($^{IMX2029}\Sigma_{(2PE+2pOH2PE)}$ = 4.5 ± 0.03 mM < $^{IMX2073}\Sigma_{(2PE+2pOH2PE)}$ = 6.2 ± 0.06 mM).

3.4. Novel strategies to improve precursor supply of the shikimate pathway

The shikimate pathway (Fig. 1) is initiated by the condensation of the two metabolite precursors phosphoenolpyruvate (PEP) and erythrose-4-phosphate (E4P). Further downstream in the shikimate pathway, a second molecule of PEP is consumed at the step of 3-phosphoshikimate 1-carboxyvinyltransferase, catalysed by Aro1. PEP is also a critical metabolite in the glycolysis, since it serves as substrate of pyruvate kinase, an enzyme that in addition to forming pyruvate is a key metabolite in both respiratory and fermentative metabolism. Furthermore, PEP is also an intermediate in *S. cerevisiae* anaplerotic functions. While investigating the reversibility of the PEP-carboxykinase (PEPCK) reaction, *PYK1* mutant alleles were identified and these mutations, although not thoroughly characterised, enabled growth on glucose of a pyruvate carboxylase *pyc1*Δ *pyc2*Δ double mutant expressing a PEPCK from *Actinobacillus succinogenes* (Zelle et al., 2010). This result suggested that the flux through pyruvate kinase was decreased. The two variant alleles of *PYK1* ($PYK1^{D147N}$ and $PYK1^{A336S}$) previously identified were reconstructed in IMX2056 (*aro3*Δ *aro8*Δ $ARO4^{K229L}$↑ $ARO7^{T226I}$↑ 3ABP↑ *TKL1*↑) by CRISPR guided *in vivo* directed mutagenesis resulting in IMX2106 (*aro3*Δ *aro8*Δ $ARO4^{K229L}$↑ $ARO7^{T226I}$↑ 3ABP↑ *TKL1*↑ $PYK1^{A336S}$) and IMX2108 (*aro3*Δ *aro8*Δ $ARO4^{K229L}$↑ $ARO7^{T226I}$↑ 3ABP↑ *TKL1*↑ $PYK1^{D147N}$). As anticipated, the disturbance of the flux through the pyruvate kinase had unwanted side effects. Both strains grew slower than the parental strain with a 17% (0.29 ± 0.00 h^{-1} vs 0.35 ± 0.00 h^{-}) and 34% (0.23 ± 0.00 h^{-1} vs 0.35 ± 0.00 h^{-1}) reduction. As already observed for strain IMX2073 ($YEN1_p$-*TYR1*), the increase in Ehrlich pathway derived aromatic alcohols seemed to be inversely correlated with the strains growth rate. The slower strain IMX2108 ($PYK1^{D147N}$) showed the best performance, producing 7.4 ± 0.04 mM of 2PE against 6.1 ± 0.16 mM for IMX2106 ($PYK1^{A336S}$) and 4.0 ± 0.01 mM for the parent IMX2056 (Fig. 6). The presence of the native *TYR1* regulation was corroborated with the production 1 mM of *p*OH2PE. To prevent the formation of the tyrosine derived higher fusel alcohol, the native *TYR1* promoters of IMX2106 and IMX2108 were replaced by the $YEN1_p$ as previously shown in strain IMX2073 ($YEN1_p$). The combination of expression of a *PYK1* mutant

Table 2
Profiling overview of genes displaying lower expression than *TYR1* and stable expression (Coefficient of variation (CV) < 15%) in a tranriptome compendium covering 55 different conditions. Expression values are the means (Avg) ± standard deviations (Std) of data from 170 GeneChip (Affymetrix YG-S98) analyses of samples issued from different steady-state chemostat cultivations (Knijnenburg et al., 2009, 2007). Expression values are expressed in Affymetrix signal units (AU).

Gene name	Systematic name	Functional description	Avg (AU)	Std (AU)	CV (%(
TYR1	YBR166C	Prephenate dehydrogenase (NADP+)	75.9	23.4	31.0
YEN1	YER041W	Similarity to DNA repair protein Rad2p and Dsh1p	31.5	5.6	18.0
AGE1	YDR524C	Similarity to hypothetical human protein and *YIL044c*	40.1	9.8	24.4
SEC18	YBR080C	Cytoplasmic ATPase involved in protein transport between ER and Golgi	62.3	15.0	24.1
MRI1	YPR118W	Similarity to *M.jannahii* translation initiation factor, eIF-2B	75.0	16.9	23.0

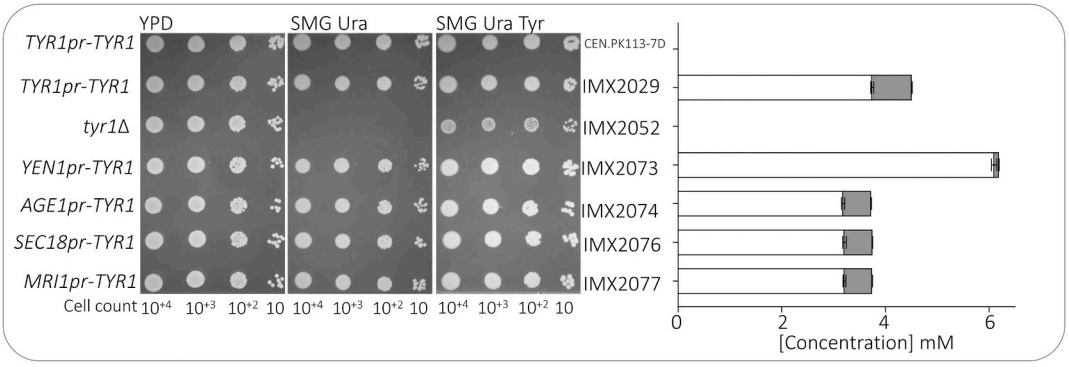

Fig. 5. Modulation of *TYR1* expression. Left panel- Spot plate assay of 2PE overproducing IMX2029 (*aro3*Δ *ARO4*^{K229L}↑ *ARO7*^{T226I}↑ 3ABP↑ *TKL1*↑), its derived progeny strains IMX2052 (*tyr1*Δ), IMX2073 (*YEN1*$_p$*-TYR1*), IMX2074 (*AGE1*$_p$*-TYR1*), IMX2076 (*SEC18*$_p$*-TYR1*) and IMX2076 (*MRI1*$_p$*-TYR1*) on YPD, SMG supplemented with 150 mg L^{-1} uracil and SMG supplemented with 150 mg L^{-1} uracil (SMG Ura) and 225 mg L^{-1} tyrosine (SMG Ura Tyr). Four different cell concentration were spotted and were incubated for 48 h (YPD) or 72 h (SMG based media) at 30 °C. Right panel- Production of 2PE (white bar), *p*OH2PE (grey bar) in (mM). Strains were grown at 30 °C for 24 h at 200 RPM in 500 mL shake flasks containing 100 mL minimal synthetic medium supplemented with 150 mg L^{-1} uracil when required and 20 g L^{-1} glucose as carbon source. The values represent averages ± mean deviations of data obtained from independent triplicate cultures.

and the down-regulated *TYR1* expression resulted in even better performance. The best combination consisted of the association of the *YEN1*$_p$*-TYR1* expression cassette with the *PYK1*^{D147N} allele. The strain IMX2124 (*aro3*Δ *aro8*Δ *ARO4*^{K229L}↑ *ARO7*^{T226I}↑ 3ABP↑ *TKL1*↑ *PYK1*^{D147N} *YEN1*$_p$*-TYR1*) reached the 10mM 2PE threshold (Fig. 6). The tuning of the flux of the pyruvate kinase by expressing mutant alleles showed to be a successful approach to increase the 2PE production in *S. cerevisiae*.

These two new impactful modifications were incrementally combined with the overexpression of the Ehrlich pathway broad substrate 2-oxo acid decarboxylase *ARO10* (IME471), the overexpression of the *E. coli* shikimate kinase *EcaroL* (Rodriguez et al., 2015) and the *ARO3*^{K222L} allele encoding a tyrosine feedback insensitive DAHP synthase (Bruckner et al., 2018; Reifenrath and Boles, 2018) (IMX2179) and finally the overexpression of *ADH2* encoding an alcohol dehydrogenase (IMX2279) (Liu et al., 2018; Wang et al., 2018). Hitherto, measurements of extracellular metabolites were performed after 24 h, a time point at which all sugars were consumed, but newly constructed strains grew slower (μ_{IME471} = 0.15 h^{-1}; $\mu_{IMX2179}$ = 0.16 h^{-1}; $\mu_{IMX2279}$ = 0.15 h^{-1}) and therefore were grown for 48 h to allow completion of all sugars. All three strains showed improvement relative to the parental strain

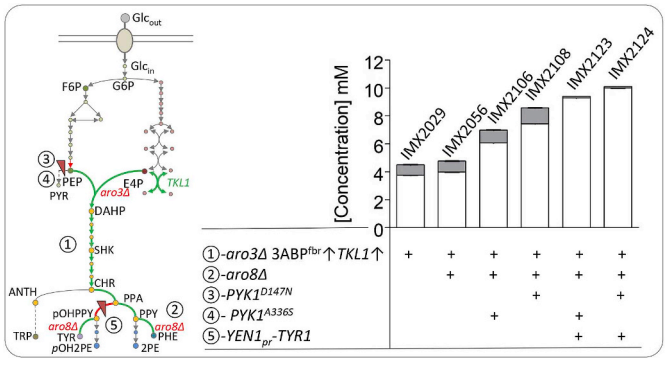

Fig. 6. Implementation of novel metabolic engineering strategies to increase 2PE production in *S. cerevisiae*. Left panel-schematic representation of the genetic modifications introduced in strains IMX2029, IMX2056, IMX2106, IMX2108, IMX2123 and IMX2124. The modifications include ① the introduction of the overexpression of the aromatic amino acid biosynthetic pathway comprising mutant alleles of *ARO4* and *ARO7,* ② the deletion of *ARO8,* ③④ the down tuning of the catalytic activity of the pyruvate kinase Pyk1 and ⑤ the alteration of *TYR1* expression. The green arrows denote an overexpression and the red arrows denotes either transcription down regulation or a reduction of the catalytic capacity of the enzyme. Right panel- Production of 2PE (white bar), *p*OH2PE (grey bar) in (mM). Strains were grown at 30 °C for 24 h at 200 RPM in 500 mL shake flasks containing 100 mL minimal synthetic medium supplemented with 150 mg L^{-1} uracil when required and 20 g L^{-1} glucose as carbon source. The values represent averages ± mean deviations of data obtained from independent triplicate cultures. + denotes the presence of a set of genetic modifications in a given strain. (For interpretation of the references to colour in this figure legend, the reader is referred to the Web version of this article.)

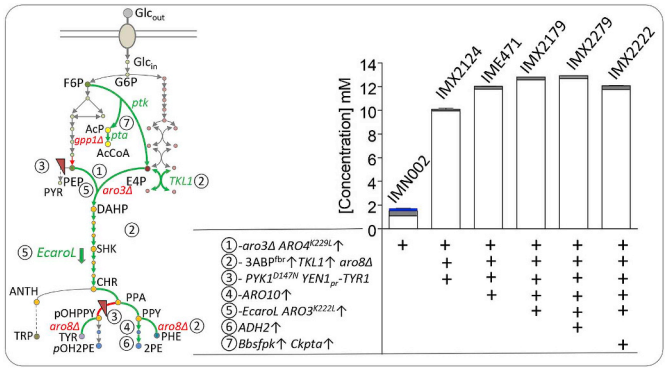

Fig. 7. Combination of strategies to increase precursors supply and overexpression of the Ehrlich pathway. Left panel-schematic representation of the genetic modifications introduced in strains IMN002, IMX2124, IME471, IMX2179, IMX2279 and IMX2222. The modifications include ①alleviation of allosteric regulation of the DAHP synthase (Aro4^{K229L}), ② the combination of the *ARO8* deletion, overexpression of the aromatic amino acid biosynthetic pathway comprising mutant alleles of *ARO4* and *ARO7* and overexpression of the transketolase Tkl1, ③ the down tuning of the catalytic activity of the pyruvate kinase Pyk1 and the alteration of *TYR1* expression, ④ overexpression of the Ehrlich pathway 2-oxo decarboxylase Aro10, ⑤ overexpression of the *E. coli* shikimate kinase EcAroL and the feedback insensitive DAHP synthase variant Aro3^{K222L}, ⑥ Overexpression of the alcohol dehydrogenase Adh2 and ⑦ expression of the heterologous phosphoketolase by-pass including the *B. brevis* phosphoketolase (*Bb*Xfpk) and a phosphotransacetylase from *C. kluyveri* (*Ck*Pta) (Bergman et al., 2016). The green arrows denote an overexpression and the red arrows denotes either transcription down regulation or a reduction of the catalytic capacity of the enzyme. Right panel- Production of 2PE (white bar), *p*OH2PE (grey bar), shikimate (blue bar) in (mM). Strains were grown at 30 °C for 48 h at 200 RPM in 500 mL shake flasks containing 100 mL minimal synthetic medium supplemented with 150 mg L^{-1} uracil when required and 20 g L^{-1} glucose as carbon source. The values represent averages ± mean deviations of data obtained from independent triplicate cultures. + denotes the presence of a or a set of genetic modifications in a given strain. (For interpretation of the references to colour in this figure legend, the reader is referred to the Web version of this article.)

IMX2124 (Fig. 7). The performances of IMX2179 and IMX2279 were undistinguishable from one another and produced the highest titre measured so far of 12.6 ± 0.3 mM and 12.7 ± 0.04 mM of 2PE, respectively.

The overexpression of *TKL1* has previously been shown to positively contribute to the production of 2PE by improving E4P supply. To further augment E4P availability to initiate the aromatic amino acid pathway, a new metabolic connection between the glycolysis and the pentose phosphate pathway was implemented. An heterologous pathway consisting of a phosphoketolase from *Bifidobacterium breve* (*Bbxfpk*) (Bergman et al., 2016) and a phosphotransacetylase from *Clostridium kluyveri* (*Ckpta*) (Meadows et al., 2016) was integrated in IMX2179 resulting in strain IMX2222. The phosphoketolase can convert fructose-6-phosphate into E4P and acetyl-phosphate redirecting a fraction of the glycolytic flux towards the pentose phosphate pathway and E4P more specifically. The acetyl-phosphate hydrolysis was shown to be reduced upon deletion of *GPP1* encoding a glycerol-3-phosphate dehydrogenase (Bergman et al., 2016). Therefore, to limit accumulation of acetate originating from acetyl-phosphate hydrolysis, the two bacterial genes were integrated at the *GPP1* locus resulting in its disruption. Additionally, the phosphotransacetylase can convert acetyl-phosphate in acetyl-CoA, which can be further used in yeast metabolism (Meadows et al., 2016). The strain IMX2222 grew faster than the parental strain ($\mu_{IMX2222} = 0.23\ h^{-1} > \mu_{IMX2179} = 0.16\ h^{-1}$), but unfortunately did not show an improvement relative to the best performing strain constructed so far: IMX2279. Instead the extracellular concentration of 2PE and total aromatics was slightly decreased by 7.2 and 6.6%, respectively.

3.5. 2PE production in controlled aerobic batch cultures

To further evaluate the influence of the new metabolic engineering solutions described in this study, we compared the performance of strains at an early and late stage of the improvement progamme (Fig. 8): the strain IMX1955 (*aro3*Δ *ARO4*^{K229L}↑ *ARO7*^{T226I}↑ 3ABP↑ *TKL1*↑) that harboured a set of modifications available at the start of the study (Curran et al., 2013; Luttik et al., 2008; Rodriguez et al., 2015), the strain IMX2179 (*aro3*Δ *aro8*Δ *ARO4*^{K229L}↑ *ARO7*^{T226I}↑ 3ABP↑ *TKL1*↑ *PYK1*^{D146N}↑ *YEN1*$_p$-*TYR1* *ARO10*↑ *EcaroL*↑ *ARO3*^{K222L}↑) the highest producing strain, which also included the metabolic engineering targets identified in this study and IMX2222 (*aro3*Δ *aro8*Δ *gpp1*Δ *ARO4*^{K229L}↑ *ARO7*^{T226I}↑ 3ABP↑ *TKL1*↑ *PYK1*^{D146N}↑ *YEN1*$_p$-*TYR1* *ARO10*↑ *EcaroL*↑ *ARO3*^{K222L}↑ *Bbxfpk*↑ *Ckpta*↑) the strain expressing the phosphoketolase-phostransactylase pathway were characterized under controlled batch conditions. The strain IMX1955 resulted from the transformation of IMX2029 with an *URA3* plasmid to restore prototrophy. The three strains along with the reference IME324 (*Spycas9*) were cultured in a 2 L batch bio-reactor with 20 g·l^{-1} glucose at a fixed pH of 5.0. In these conditions (aerobic and glucose excess), *S. cerevisiae* predominantly metabolizes glucose through fermentation metabolism (de Deken, 1966; Van Hoek et al., 1998) and exhibits a diauxic growth profile. As expected, IME324 did not produce any fusel alcohols or intermediates of the shikimate pathway when grown in these conditions. The strain had a growth rate of 0.35 h^{-1} (Table 3) and was completing ethanol consumption in a typical diauxic shift (Fig. 8). The intermediate 2PE producing strain IMX1955 produced 4.42 ± 0.25 mM of 2PE in 30 h. The best 2PE producing strain IMX2179 grew even slower with a growth rate 0.1 h^{-1} but produced 12.7 ± 0.25 mM of 2PE in 40 h. Interestingly IMX2179 showed a 88% reduction in *p*OH2PE ($[pOH2PE]_{IMX2179} = 0.172 \pm 0.00$ mM vs $[pOH2PE]_{IMX1955} = 1.38 \pm 0.01$ Mm) confirming the positive effect of downregulating the prephenate dehydrogenase *TYR1* gene. Conversely to what was observed in shake flask cultures the strain IMX2179 produced 1 mM PPY (phenylpyruvate) (Fig. 8). In these conditions the 2PE yield on glucose of the strain IMX2179 was calculated to be of 0.113 ± 0.002 mol mol^{-1} (Table 3) which represents nearly one quarter of the 2PE maximum theoretical yield on glucose (0.500 mol mol^{-1} or 0.339 g/g). In line with the shake flask results, the strain IMX2222 showed reduced performance compared to IMX2179. But contrasting with the shake flask cultures, this strain grew much slower in a controlled bioreactor than in shake flask (0.06 ± 0.00 h^{-1} versus 0.23 + 0.00 h^{-1}). Additionally, IMX2179 and IMX2222 displayed an unusual growth profile, the off-gas CO_2 profile (Fig. S1), revealed that the growth phase on glucose was not steady including three distinct phases. After an initial growth phase, the culture slowed down before resuming exponential growth. In both cases, the glucose phase was followed by a

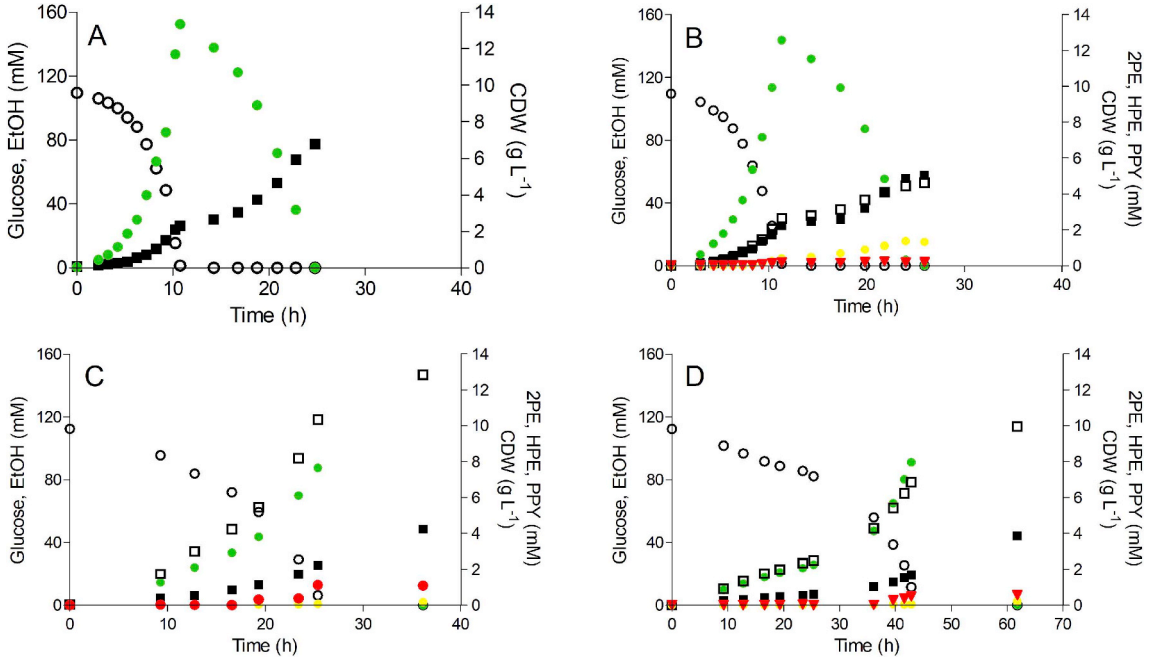

Fig. 8. Product formation of the 2PE-producing strains *S. cerevisiae* IMX1955, IMX2179, IMX2222 and the control strain IME324 in bioreactors. Growth and extracellular metabolites formation were studied in aerobic and pH controlled (pH 5.0) batch cultures on glucose. The results shown are from a single representative experiment. Panel A: IME324, panel B: IMX1955, panel C: IMX2179 and panel D: IMX2222. ■ Cell dry weight (g L^{-1}), □ 2PE, ◯ glucose, ● ethanol, ● pOH2PE, ● pHOPPY (mM).

Table 3
Fermentation performance indicators of 2PE producing strains. Specifc growth rate (μ), yields (Y) of biomass (X) and ethanol (EtOH) on glucose (S) and yield (Y) of biomass, 2-phenylethanol (2PE), *p*-hydroxyphenylethanol (*p*OH2PE) and phenylpyruvate (PPY) on glucose in aerobic bioreactor batch cultures of *S. cerevisiae* strains IME324 (control strain), IMX1955, IMX2179 and IMX2222 carrying several genetic modifications for increased 2PE production.

Strain	IME324	IMX1955	IMX2179	IMX2222
Relevant genotype	*cas9*	*cas9 aro3Δ aro8Δ 3ABP^{fbr}↑ TKL1↑*	*cas9 aro3Δ aro8Δ 3ABP^{fbr}↑ TKL1↑ PYK1^{D146N} YEN1$_p$-TYR1 ARO10↑ EcaroL↑ ARO3^{K222L}↑*	*cas9 aro3Δ aro8Δ gpp1Δ 3ABP^{fbr}↑ TKL1↑ PYK1^{D146N} YEN1$_p$-TYR1 ARO10↑ EcaroL↑ ARO3^{K222L}↑ Bbxfpk↑ Ckpta↑*
[a]μ_{max} (h^{-1})	0.35 ± 0.06	0.30 ± 0.01	0.10 ± 0.01	0.06 ± 0.00
[a]$Y_{X/S}$ (g g^{-1})	0.12 ± 0.00	0.11 ± 0.00	0.11 ± 0.00	0.09 ± 0.00
[a]$Y_{EtOH/S}$ (mol mol^{-1})	1.41 ± 0.00	1.33 ± 0.00	0.81 ± 0.02	0.88 ± 0.03
$Y_{X/S}$ (g g^{-1})	0.34 ± 0.00	0.26 ± 0.01	0.21 ± 0.00	0.18 ± 0.01
$Y_{2PE/S}$ (mol mol^{-1})	–	0.04 ± 0.00	0.11 ± 0.00	0.09 ± 0.00
$Y_{pOH2PE/S}$ (mol mol^{-1})	–	0.01 ± 0.00	0.002 ± 0.00	0.002 ± 0.000
$Y_{PPY/S}$ (mol mol^{-1})	–	0.002 ± 0.00	0.01 ± 0.00	0.005 ± 0.000

[a] Determined from the glucose phase only.

diauxic ethanol phase. Although showing similar CO_2 profiles, IMX2222 exhibited an elongated growth phase twice longer that of IMX2179.

4. Discussion

Hitherto, metabolic engineering strategies devised to improve the production of aromatic metabolites derived from the three aromatic amino acids were axed around the relief of regulatory constraints of the shikimate pathway (Koopman et al., 2012; Rodriguez et al., 2015). Indeed as most of the amino acid biosynthetic pathways, the phenylalanine, tyrosine and tryptophan biosynthetic routes are tightly regulated at transcriptional and (post)-translational levels (Helmstaedt et al., 2005; Schnappauf et al., 1998a, 1998b). The alleviation of the metabolic control of the DAHP synthase and chorismate mutase was proven to be key to unlock the production of metabolites derived from the shikimate pathway (Luttik et al., 2008). Furthermore the relief of the native transcriptional control by overexpression of the genes of the shikimate pathway led to the construction of the best aromatic compounds (phenylpropanoids, flavonoids, alkaloids) producers so far (Eichenberger et al., 2018; Gottardi et al., 2017a; Hawkins and Smolke, 2008; Levisson et al., 2018). Although well-established, these approaches were applied to produce compounds downstream of phenylalanine, but not phenylethanol which represents a by-product for the formation of these compounds. In line with these previous works, the relief of allosteric and transcriptional regulation of the shikimate pathway positively impacted the formation of 2PE. While these modifications led to an increase in catalytic capacity of the pathway, our study more specifically focused on the augmentation of the supply of the DAHP synthase substrates, PEP and E4P and elimination of metabolic by-products.

Firstly, improving PEP supply by tuning pyruvate kinase activity ended successfully. Earlier attempts to improve PEP supply for tyrosine biosynthesis by lowering *PYK1* expression or expressing specific mutant contrastingly did not lead to any improvement but instead showed to negatively impact the aromatic amino acid synthesis (Gold et al., 2015). Also the phenotype of the strains carrying the *PYK1*^{D147N} allele used in this study suggests a weakening of the kinase activity (Zelle et al., 2010), that might lead to an increase in intracellular PEP concentration. The exact reasons at the origin of this improvement remains uncharacterized and further work such as in vitro enzymatic activity measurements or intracellular metabolites quantification will be necessary to provide a full explanation.

Conversely, the second approach consisting in the diversion of a fraction of the glycolytic flux into the non-oxidative branch of the pentose pathway by expressing a phosphoketolase (*Bb*Xfpk) -phosphotransacetylase (*CkPta*) pathway did not result in an increase of Ehrlich higher alcohol biosynthesis. Phosphoketolase does not only hydrolyze fructose-6-phosphate (C6) into erythrose-4-phosphate (E4P) and acetyl-phosphaste. Most of these enzymes including the *Bifidobacterium breve* phosphoketolase exhibit higher activity with xylyulose-5-phosphate (Bergman et al., 2016). The significant accumulation of acetate in IMX222 culture supernatant supported the functionality of the *Bifidobacterium* shunt (Fleige et al., 2011; Suzuki et al., 2010), despite the deletion of *GPP1* that prevents the excessive endogenous hydrolysis of acetyl-phosphate (Bergman et al., 2016). The absence of improvement might be associated with too low fructose-6-phosphate (F6P) intracellular concentration. Several genetic modifications have been already shown to affect intracellular F6P concentration, such as deletion of one of the two phosphofructokinases, *PFK1* or *PFK2* (Boles et al., 1993) or deletion of one of the 6-phosphofructo-2-kinases, *PFK26/PFK27*, that catalyze the conversion of F6P to fructose-2,6-biphosphate (Boles et al., 1996). Implementation of these changes in IMX2222 could yield F6P concentration compatible with the full expression the metabolic potential of the *Bifidobacterium* shunt and eventually higher 2PE concentration.

While in shake flask the strain IMX2222 exhibited a better 2PE productivity than IMX2179, these results were reversed in bioreactors. Both strains displayed a reduced growth rate but this phenotype was exacerbated in IMX2222 (Fig. 8 and Fig. S1). Controlled bioreactors conversely to shake flasks are sparged with pressurized air stripping produced carbon dioxide. The *PYK1* mutations applied in this study arose during evolution in a pyruvate carboxylase negative strain (*pyc1Δ pyc2Δ*) expressing a phosphoenolpyruvate carboxykinase (PEPCK) of *Actinobacillus succinogenes* to enable a sufficiently high anaplerotic flux to sustain growth (Zelle et al., 2010). In these strains growth was only observed in strains carrying either of the *PYK1* mutations under high CO_2 concentrations. The thermodynamic potential of carboxylation reactions is enhanced under a CO_2 rich atmosphere. The *PYK1*^{D146N} mutation has been engineered in both IMX2179 and IMX2222. The resulting decrease in pyruvate levels affects the maximal growth rate but could potentially also result in a lowered anaplerotic flux through Pyc1, Pyc2 and Mae1. These enzymes would favour from increased CO_2 conditions. Lower initial CO_2 and pyruvate levels might be detrimental as these strains might be unable to produce sufficient CO_2 and pyruvate derived metabolites required for biosynthetic reactions and fast growth. This effect could be even stronger for IMX2222 because the phosphoketolase diverts even more carbon away from pyruvate.

The points discussed so far have implications beyond 2PE production as these strategies could be applied to the biosynthesis of a wide range of products that are based on the aromatic amino acid carbon skeleton. In contrast metabolic engineering strategies aiming at the elimination of the by-product *p*OH2PE biosynthesis are limited to 2PE.

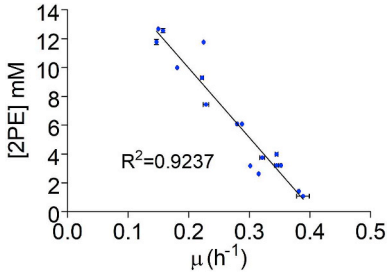

Fig. 9. Correlation between growth rate and extracellularly produced 2PE in metabolically engineered *S. cerevisiae* strains. Data plotted in this graph correspond to the 2PE concentrations reported in Figures and the strain growth rates measured in the same experiments (Tables S.3 and S.4). The plotted values represent averages ± mean deviations of data obtained from independent triplicate cultures. The R^2 value represents the correlation coefficient of the linear regression through the data points. The line shows a Y-intercept of 19.6 mM which simulates full growth inhibition.

The activation of the Ehrlich pathway indiscriminately stimulates the formation of all fusel alcohols and acids (Hazelwood et al., 2008; Kim et al., 2014; Luttik et al., 2008; Romagnoli et al., 2012, 2015; Shen et al., 2016). While the fusel acids phenylacetate (PAA) and *p*-hydroxyphenylacetate (*p*OHPAA) were systematically absent, we could not exclude the presence of tryptophol (*aka*. indole-3-ethanol), the Ehrlich alcohol derived from tryptophan. If trytophol production occured, a similar approach that of applied for *TYR1* could be applied at the chorismate node by down-regulating the anthranilate synthase genes *TRP2* and *TRP3*.

The best engineered strains were able to produce up to 12 .7 mM of 2PE but exhibited a strong reduction up to 75% in growth rate relative to the lineage parental strains CEN.PK113-7D or IMX581 (Table 3, Fig. 8). This growth decrease was systematically observed in intermediate strains. Remarkably, these two strain characteristics were near perfectly inversely correlated (Coefficient of correlation R^2 = 0.9237) (Fig. 9). This linear model predicts a complete growth inhibition around 19.4 mM of 2PE, a value in line with 2PE inhibitory concentration found in literature that are comprised between 10 and 25mM (Hazelwood et al., 2006). This effect could be anticipated as 2PE has a partition coefficient octanol/water ($LogP_{O/W}$) of 1.36 denoting lipophilic characteristics. This is in agreement with some of the proposed 2PE toxicity mechanisms, such as increasing membrane fluidity (Ingram and Buttke, 1984) that consequently would cause leakage of ions (Seward et al., 1996), a reduced uptake of nutrients such as glucose and amino acids (Lester, 1965) and a reduction of the respiratory capacity, possibly due to changes in mitochondrial membrane fluidity (Stark et al., 2003).

Therefore, considering this toxicity further improvement of the 2PE yield on glucose ($Y_{2PE/S}$) to approach the maximum theoretical yield of 0.500 mol mol^{-1} will certainly require the addition of operational unit such as *in situ* product recovery techniques to continuously remove the product from the broth to prevent its toxicity. The strain performances reported in this study are the highest titres of 2PE ever achieved *de novo* in *S. cerevisiae* or any other Saccharomycotina yeasts (Wang et al., 2019). Furthermore, the strain IMX2179 can be used as platform for the development of the next 2PE producing strain generation.

Financial support

This project has received funding from the European Union's Horizon 2020 research and innovation program under grant agreement No 720824

Declaration of interest

None.

Acknowledgements

We would like to thank Dr John Morrissey and Dr Arun Rajkumar for fruitful discussion. We would like to thank Mr Erik de Hulster for the supervision of the fermentation and Francine Boonekamp for providing template plasmids for the construction of promoter and terminator parts.

Appendix A. Supplementary data

Supplementary data to this article can be found online at https://doi.org/10.1016/j.ymben.2019.09.011.

References

Ball, S.G., Wickner, R.B., Cottarel, G., Schaus, M., Tirtiaux, C., 1986. Molecular cloning and characterization of *ARO7-OSM2*, a single yeast gene necessary for chorismate mutase activity and growth in hypertonic medium. Mol. Gen. Genet. 205, 326–330. https://doi.org/10.1007/bf00430446.

Bergman, A., Siewers, V., Nielsen, J., Chen, Y., 2016. Functional expression and evaluation of heterologous phosphoketolases in *Saccharomyces cerevisiae*. Amb. Express 6, 115. https://doi.org/10.1186/s13568-016-0290-0.

Boer, V.M., Tai, S.L., Vuralhan, Z., Arifin, Y., Walsh, M.C., Piper, M.D., de Winde, J.H., Pronk, J.T., Daran, J.M., 2007. Transcriptional responses of *Saccharomyces cerevisiae* to preferred and nonpreferred nitrogen sources in glucose-limited chemostat cultures. FEMS Yeast Res. 7, 604–620. https://doi.org/10.1111/j.1567-1364.2007.00220.x.

Boles, E., Gohlmann, H.W., Zimmermann, F.K., 1996. Cloning of a second gene encoding 5-phosphofructo-2-kinase in yeast, and characterization of mutant strains without fructose-2,6-bisphosphate. Mol. Microbiol. 20, 65–76. https://doi.org/10.1111/j.1365-2958.1996.tb02489.x.

Boles, E., Heinisch, J., Zimmermann, F.K., 1993. Different signals control the activation of glycolysis in the yeast *Saccharomyces cerevisiae*. Yeast 9, 761–770. https://doi.org/10.1002/yea.320090710.

Boonekamp, F.J., Dashko, S., van den Broek, M., Gehrmann, T., Daran, J.M., Daran-Lapujade, P., 2018. The genetic makeup and expression of the glycolytic and fermentative pathways are highly conserved within the *Saccharomyces* genus. Front. Genet. 9, 504. https://doi.org/10.3389/fgene.2018.00504.

Bruckner, C., Oreb, M., Kunze, G., Boles, E., Tripp, J., 2018. An expanded enzyme toolbox for production of cis, cis-muconic acid and other shikimate pathway derivatives in *Saccharomyces cerevisiae*. FEMS Yeast Res. 18. https://doi.org/10.1093/femsyr/foy017.

Cordente, A.G., Schmidt, S., Beltran, G., Torija, M.J., Curtin, C.D., 2019. Harnessing yeast metabolism of aromatic amino acids for fermented beverage bioflavouring and bioproduction. Appl. Microbiol. Biotechnol. 103, 4325–4336. https://doi.org/10.1007/s00253-019-09840-w.

Curran, K.A., Leavitt, J.M., Karim, A.S., Alper, H.S., 2013. Metabolic engineering of muconic acid production in *Saccharomyces cerevisiae*. Metab. Eng. 15, 55–66. https://doi.org/10.1016/j.ymben.2012.10.003.

de Deken, R.H., 1966. The crabtree effect: a regulatory system in yeast. Microbiology 44, 149–156. https://doi.org/10.1099/00221287-44-2-149.

de Kok, S., Yilmaz, D., Suir, E., Pronk, J.T., Daran, J.M., van Maris, A.J., 2011. Increasing free-energy (ATP) conservation in maltose-grown *Saccharomyces cerevisiae* by expression of a heterologous maltose phosphorylase. Metab. Eng. 13, 518–526. https://doi.org/10.1016/j.ymben.2011.06.001.

DiCarlo, J.E., Norville, J.E., Mali, P., Rios, X., Aach, J., Church, G.M., 2013. Genome engineering in *Saccharomyces cerevisiae* using CRISPR-Cas systems. Nucleic Acids Res. 41, 4336–4343. https://doi.org/10.1093/nar/gkt135.

Dickinson, J.R., Salgado, L.E., Hewlins, M.J., 2003. The catabolism of amino acids to long chain and complex alcohols in *Saccharomyces cerevisiae*. J. Biol. Chem. 278, 8028–8034. https://doi.org/10.1074/jbc.M211914200.

Duncan, K., Edwards, R.M., Coggins, J.R., 1988. The *Saccharomyces cerevisiae* ARO1 gene. An example of the co-ordinate regulation of five enzymes on a single biosynthetic pathway. FEBS Lett. 241, 83–88. https://doi.org/10.1016/0014-5793(88)81036-6.

Ehrlich, F., 1907. Über die Bedingungen der Fuselölbildung und über ihren Zusammenhang mit dem Eiweißaufbau der Hefe. Ber. Dtsch. Chem. Ges. 40, 1027–1047. https://doi.org/10.1002/cber.190704001156.

Eichenberger, M., Hansson, A., Fischer, D., Durr, L., Naesby, M., 2018. De novo biosynthesis of anthocyanins in *Saccharomyces cerevisiae*. FEMS Yeast Res. 18. https://doi.org/10.1093/femsyr/foy046.

Eikani, M.H., Golmohammad, F., Rowshanzamir, S., Mirza, M., 2005. Recovery of water-soluble constituents of rose oil using simultaneous distillation–extraction. Flavour Fragrance J. 20, 555–558. https://doi.org/10.1002/ffj.1482.

Entian, K.-D., Kötter, P., 2007. 25 yeast genetic strain and plasmid collections. In: In: Stansfield, I., Stark, M.J.R. (Eds.), Methods in Microbiology, vol.36. Academic Press, pp. 629–666.

Eshkol, N., Sendovski, M., Bahalul, M., Katz-Ezov, T., Kashi, Y., Fishman, A., 2009. Production of 2-phenylethanol from L-phenylalanine by a stress tolerant *Saccharomyces cerevisiae* strain. J. Appl. Microbiol. 106, 534–542. https://doi.org/10.1111/j.1365-2672.2008.04023.x.

Etschmann, M.M., Bluemke, W., Sell, D., Schrader, J., 2002. Biotechnological production of 2-phenylethanol. Appl. Microbiol. Biotechnol. 59, 1–8. https://doi.org/10.1007/

s00253-002-0992-x.
Etschmann, M.M., Schrader, J., 2006. An aqueous-organic two-phase bioprocess for efficient production of the natural aroma chemicals 2-phenylethanol and 2-phenylethylacetate with yeast. Appl. Microbiol. Biotechnol. 71, 440–443. https://doi.org/10.1007/s00253-005-0281-6.
Fleige, C., Kroll, J., Steinbuchel, A., 2011. Establishment of an alternative phosphoketolase-dependent pathway for fructose catabolism in Ralstonia eutropha H16. Appl. Microbiol. Biotechnol. 91, 769–776. https://doi.org/10.1007/s00253-011-3284-5.
Galanie, S., Thodey, K., Trenchard, I.J., Filsinger Interrante, M., Smolke, C.D., 2015. Complete biosynthesis of opioids in yeast. Science 349, 1095–1100. https://doi.org/10.1126/science.aac9373.
Gold, N.D., Gowen, C.M., Lussier, F.X., Cautha, S.C., Mahadevan, R., Martin, V.J., 2015. Metabolic engineering of a tyrosine-overproducing yeast platform using targeted metabolomics. Microb. Cell Factories 14, 73. https://doi.org/10.1186/s12934-015-0252-2.
Gottardi, M., Grun, P., Bode, H.B., Hoffmann, T., Schwab, W., Oreb, M., Boles, E., 2017a. Optimisation of trans-cinnamic acid and hydrocinnamyl alcohol production with recombinant *Saccharomyces cerevisiae* and identification of cinnamyl methyl ketone as a by-product. FEMS Yeast Res. 17. https://doi.org/10.1093/femsyr/fox091.
Gottardi, M., Knudsen, J.D., Prado, L., Oreb, M., Branduardi, P., Boles, E., 2017b. De novo biosynthesis of trans-cinnamic acid derivatives in *Saccharomyces cerevisiae*. Appl. Microbiol. Biotechnol. 101, 4883–4893. https://doi.org/10.1007/s00253-017-8220-x.
Hawkins, K.M., Smolke, C.D., 2008. Production of benzylisoquinoline alkaloids in *Saccharomyces cerevisiae*. Nat. Chem. Biol. 4, 564–573. https://doi.org/10.1038/nchembio.105.
Hazelwood, L.A., Daran, J.M., van Maris, A.J., Pronk, J.T., Dickinson, J.R., 2008. The Ehrlich pathway for fusel alcohol production: a century of research on *Saccharomyces cerevisiae* metabolism. Appl. Environ. Microbiol. 74, 2259–2266. https://doi.org/10.1128/AEM.02625-07.
Hazelwood, L.A., Tai, S.L., Boer, V.M., de Winde, J.H., Pronk, J.T., Daran, J.M., 2006. A new physiological role for Pdr12p in *Saccharomyces cerevisiae*: export of aromatic and branched-chain organic acids produced in amino acid catabolism. FEMS Yeast Res. 6, 937–945. https://doi.org/10.1111/j.1567-1364.2006.00094.x.
Helmstaedt, K., Heinrich, G., Lipscomb, W.N., Braus, G.H., 2002. Refined molecular hinge between allosteric and catalytic domain determines allosteric regulation and stability of fungal chorismate mutase. Proc. Natl. Acad. Sci. U. S. A. 99, 6631–6636. https://doi.org/10.1073/pnas.092130899.
Helmstaedt, K., Strittmatter, A., Lipscomb, W.N., Braus, G.H., 2005. Evolution of 3-deoxy-D-arabino-heptulosonate-7-phosphate synthase-encoding genes in the yeast *Saccharomyces cerevisiae*. Proc. Natl. Acad. Sci. U. S. A. 102, 9784–9789. https://doi.org/10.1073/pnas.0504238102.
Ingram, L.O., Buttke, T.M., 1984. Effects of alcohols on micro-organisms. Adv. Microb. Physiol. 25, 253–300.
Iraqui, I., Vissers, S., Andre, B., Urrestarazu, A., 1999. Transcriptional induction by aromatic amino acids in *Saccharomyces cerevisiae*. Mol. Cell. Biol. 19, 3360–3371. https://doi.org/10.1128/mcb.19.5.3360.
Iraqui, I., Vissers, S., Cartiaux, M., Urrestarazu, A., 1998. Characterisation of *Saccharomyces cerevisiae ARO8* and *ARO9* genes encoding aromatic aminotransferases I and II reveals a new aminotransferase subfamily. Mol. Gen. Genet. 257, 238–248. https://doi.org/10.1007/s004380050644.
Jones, D.G., Reusser, U., Braus, G.H., 1991. Molecular cloning, characterization and analysis of the regulation of the *ARO2* gene, encoding chorismate synthase, of *Saccharomyces cerevisiae*. Mol. Microbiol. 5, 2143–2152. https://doi.org/10.1111/j.1365-2958.1991.tb02144.x.
Kim, B., Cho, B.R., Hahn, J.S., 2014. Metabolic engineering of *Saccharomyces cerevisiae* for the production of 2-phenylethanol via Ehrlich pathway. Biotechnol. Bioeng. 111, 115–124. https://doi.org/10.1002/bit.24993.
Knijnenburg, T.A., Daran, J.M., van den Broek, M.A., Daran-Lapujade, P.A., de Winde, J.H., Pronk, J.T., Reinders, M.J., Wessels, L.F., 2009. Combinatorial effects of environmental parameters on transcriptional regulation in *Saccharomyces cerevisiae*: a quantitative analysis of a compendium of chemostat-based transcriptome data. BMC Genomics 10, 53. https://doi.org/10.1186/1471-2164-10-53.
Knijnenburg, T.A., de Winde, J.H., Daran, J.M., Daran-Lapujade, P., Pronk, J.T., Reinders, M.J., Wessels, L.F., 2007. Exploiting combinatorial cultivation conditions to infer transcriptional regulation. BMC Genomics 8, 25. https://doi.org/10.1186/1471-2164-8-25.
Koopman, F., Beekwilder, J., Crimi, B., van Houwelingen, A., Hall, R.D., Bosch, D., van Maris, A.J., Pronk, J.T., Daran, J.M., 2012. De novo production of the flavonoid naringenin in engineered *Saccharomyces cerevisiae*. Microb. Cell Factories 11, 155. https://doi.org/10.1186/1475-2859-11-155.
Kuijpers, N.G., Solis-Escalante, D., Bosman, L., van den Broek, M., Pronk, J.T., Daran, J.M., Daran-Lapujade, P., 2013. A versatile, efficient strategy for assembly of multi-fragment expression vectors in *Saccharomyces cerevisiae* using 60 bp synthetic recombination sequences. Microb. Cell Factories 12, 47. https://doi.org/10.1186/1475-2859-12-47.
Lee, M.E., DeLoache, W.C., Cervantes, B., Dueber, J.E., 2015. A highly characterized yeast toolkit for modular, multipart assembly. ACS Synth. Biol. 4, 975–986. https://doi.org/10.1021/sb500366v.
Lester, G., 1965. Inhibition of growth, synthesis, and permeability in neurospora crassa by phenethyl alcohol. J. Bacteriol. 90, 29–37.
Levisson, M., Patinios, C., Hein, S., de Groot, P.A., Daran, J.M., Hall, R.D., Martens, S., Beekwilder, J., 2018. Engineering de novo anthocyanin production in *Saccharomyces cerevisiae*. Microb. Cell Factories 17, 103. https://doi.org/10.1186/s12934-018-0951-6.
Libkind, D., Hittinger, C.T., Valerio, E., Goncalves, C., Dover, J., Johnston, M., Goncalves, P., Sampaio, J.P., 2011. Microbe domestication and the identification of the wild genetic stock of lager-brewing yeast. Proc. Natl. Acad. Sci. U. S. A. 108, 14539–14544. https://doi.org/10.1073/pnas.1105430108.
Liu, C., Zhang, K., Cao, W., Zhang, G., Chen, G., Yang, H., Wang, Q., Liu, H., Xian, M., Zhang, H., 2018. Genome mining of 2-phenylethanol biosynthetic genes from Enterobacter sp. CGMCC 5087 and heterologous overproduction in Escherichia coli. Biotechnol. Biofuels 11, 305. https://doi.org/10.1186/s13068-018-1297-3.
Longo, M., Sanromán, M., 2006. Production of food aroma compounds: microbial and enzymatic methodologies. Food Technol. Biotechnol. 44, 335–353.
Lopes, C.A., Barrio, E., Querol, A., 2010. Natural hybrids of S. cerevisiae x S. kudriavzevii share alleles with European wild populations of Saccharomyces kudriavzevii. FEMS Yeast Res. 10, 412–421. https://doi.org/10.1111/j.1567-1364.2010.00614.x.
Luttik, M.A., Kotter, P., Salomons, F.A., van der Klei, I.J., van Dijken, J.P., Pronk, J.T., 2000. The *Saccharomyces cerevisiae* ICL2 gene encodes a mitochondrial 2-methylisocitrate lyase involved in propionyl-coenzyme A metabolism. J. Bacteriol. 182, 7007–7013. https://doi.org/10.1128/jb.182.24.7007-7013.2000.
Luttik, M.A., Vuralhan, Z., Suir, E., Braus, G.H., Pronk, J.T., Daran, J.M., 2008. Alleviation of feedback inhibition in *Saccharomyces cerevisiae* aromatic amino acid biosynthesis: quantification of metabolic impact. Metab. Eng. 10, 141–153. https://doi.org/10.1016/j.ymben.2008.02.002.
Mans, R., van Rossum, H.M., Wijsman, M., Backx, A., Kuijpers, N.G., van den Broek, M., Daran-Lapujade, P., Pronk, J.T., van Maris, A.J., Daran, J.M., 2015. CRISPR/Cas9: a molecular Swiss army knife for simultaneous introduction of multiple genetic modifications in *Saccharomyces cerevisiae*. FEMS Yeast Res. 15. https://doi.org/10.1093/femsyr/fov004.
Mans, R., Wijsman, M., Daran-Lapujade, P., Daran, J.M., 2018. A protocol for introduction of multiple genetic modifications in *Saccharomyces cerevisiae* using CRISPR/Cas9. FEMS Yeast Res. 18. https://doi.org/10.1093/femsyr/foy063.
Meadows, A.L., Hawkins, K.M., Tsegaye, Y., Antipov, E., Kim, Y., Raetz, L., Dahl, R.H., Tai, A., Mahatdejkul-Meadows, T., Xu, L., Zhao, L., Dasika, M.S., Murarka, A., Lenihan, J., Eng, D., Leng, J.S., Liu, C.-L., Wenger, J.W., Jiang, H., Chao, L., Westfall, P., Lai, J., Ganesan, S., Jackson, P., Mans, R., Platt, D., Reeves, C.D., Saija, P.R., Wichmann, G., Holmes, V.F., Benjamin, K., Hill, P.W., Gardner, T.S., Tsong, A.E., 2016. Rewriting yeast central carbon metabolism for industrial isoprenoid production. Nature 537, 694. https://doi.org/10.1038/nature19769. https://www.nature.com/articles/nature19769#supplementary-information.
Papapetridis, I., Goudriaan, M., Vazquez Vitali, M., de Keijzer, N.A., van den Broek, M., van Maris, A.J.A., Pronk, J.T., 2018. Optimizing anaerobic growth rate and fermentation kinetics in *Saccharomyces cerevisiae* strains expressing Calvin-cycle enzymes for improved ethanol yield. Biotechnol. Biofuels 11, 17. https://doi.org/10.1186/s13068-017-1001-z.
Papapetridis, I., van Dijk, M., van Maris, A.J.A., Pronk, J.T., 2017. Metabolic engineering strategies for optimizing acetate reduction, ethanol yield and osmotolerance in *Saccharomyces cerevisiae*. Biotechnol. Biofuels 10, 107. https://doi.org/10.1186/s13068-017-0791-3.
Piper, M.D., Daran-Lapujade, P., Bro, C., Regenberg, B., Knudsen, S., Nielsen, J., Pronk, J.T., 2002. Reproducibility of oligonucleotide microarray transcriptome analyses. An interlaboratory comparison using chemostat cultures of *Saccharomyces cerevisiae*. J. Biol. Chem. 277, 37001–37008. https://doi.org/10.1074/jbc.M204490200.
Pronk, J.T., 2002. Auxotrophic yeast strains in fundamental and applied research. Appl. Environ. Microbiol. 68, 2095–2100. https://doi.org/10.1128/aem.68.5.2095-2100.2002.
Reifenrath, M., Bauer, M., Oreb, M., Boles, E., 2018. Bacterial bifunctional chorismate mutase-prephenate dehydratase PheA increases flux into the yeast phenylalanine pathway and improves mandelic acid production. Metab Eng Commun 7, e00079. https://doi.org/10.1016/j.mec.2018.e00079.
Reifenrath, M., Boles, E., 2018. Engineering of hydroxymandelate synthases and the aromatic amino acid pathway enables de novo biosynthesis of mandelic and 4-hydroxymandelic acid with *Saccharomyces cerevisiae*. Metab. Eng. 45, 246–254. https://doi.org/10.1016/j.ymben.2018.01.001.
Rodriguez, A., Kildegaard, K.R., Li, M., Borodina, I., Nielsen, J., 2015. Establishment of a yeast platform strain for production of p-coumaric acid through metabolic engineering of aromatic amino acid biosynthesis. Metab. Eng. 31, 181–188. https://doi.org/10.1016/j.ymben.2015.08.003.
Rodriguez, A., Strucko, T., Stahlhut, S.G., Kristensen, M., Svenssen, D.K., Forster, J., Nielsen, J., Borodina, I., 2017. Metabolic engineering of yeast for fermentative production of flavonoids. Bioresour. Technol. 245, 1645–1654. https://doi.org/10.1016/j.biortech.2017.06.043.
Romagnoli, G., Knijnenburg, T.A., Liti, G., Louis, E.J., Pronk, J.T., Daran, J.M., 2015. Deletion of the *Saccharomyces cerevisiae ARO8* gene, encoding an aromatic amino acid transaminase, enhances phenylethanol production from glucose. Yeast 32, 29–45. https://doi.org/10.1002/yea.3015.
Romagnoli, G., Luttik, M.A., Kotter, P., Pronk, J.T., Daran, J.M., 2012. Substrate specificity of thiamine pyrophosphate-dependent 2-oxo-acid decarboxylases in *Saccharomyces cerevisiae*. Appl. Environ. Microbiol. 78, 7538–7548. https://doi.org/10.1128/AEM.01675-12.
Schnappauf, G., Krappmann, S., Braus, G.H., 1998a. Tyrosine and tryptophan act through the same binding site at the dimer interface of yeast chorismate mutase. J. Biol. Chem. 273, 17012–17017. https://doi.org/10.1074/jbc.273.27.17012.
Schnappauf, G., Lipscomb, W.N., Braus, G.H., 1998b. Separation of inhibition and activation of the allosteric yeast chorismate mutase. Proc. Natl. Acad. Sci. U. S. A. 95, 2868–2873. https://doi.org/10.1073/pnas.95.6.2868.
Seward, R., Willetts, J.C., Dinsdale, M.G., Lloyd, D., 1996. The effects OF ethanol, HEXAN-1-OL, and 2-PHENYLETHANOL ON cider yeast growth, viability, and energy status; synergistic inhibition. J. Inst. Brew. 102, 439–443. https://doi.org/10.1002/j.2050-0416.1996.tb00928.x.

Shen, L., Nishimura, Y., Matsuda, F., Ishii, J., Kondo, A., 2016. Overexpressing enzymes of the Ehrlich pathway and deleting genes of the competing pathway in *Saccharomyces cerevisiae* for increasing 2-phenylethanol production from glucose. J. Biosci. Bioeng. 122, 34–39. https://doi.org/10.1016/j.jbiosc.2015.12.022.

Shin, S.Y., Han, N.S., Park, Y.C., Kim, M.D., Seo, J.H., 2011. Production of resveratrol from p-coumaric acid in recombinant *Saccharomyces cerevisiae* expressing 4-coumarate:coenzyme A ligase and stilbene synthase genes. Enzym. Microb. Technol. 48, 48–53. https://doi.org/10.1016/j.enzmictec.2010.09.004.

Stark, D., Munch, T., Sonnleitner, B., Marison, I.W., von Stockar, U., 2002. Extractive bioconversion of 2-phenylethanol from L-phenylalanine by *Saccharomyces cerevisiae*. Biotechnol. Prog. 18, 514–523. https://doi.org/10.1021/bp020006n.

Stark, D., Zala, D., Münch, T., Sonnleitner, B., Marison, I.W., von Stockar, U., 2003. Inhibition aspects of the bioconversion of l-phenylalanine to 2-phenylethanol by *Saccharomyces cerevisiae*. Enzym. Microb. Technol. 32, 212–223. https://doi.org/10.1016/S0141-0229(02)00237-5.

Strucko, T., Buron, L.D., Jarczynska, Z.D., Nodvig, C.S., Molgaard, L., Halkier, B.A., Mortensen, U.H., 2017. CASCADE, a platform for controlled gene amplification for high, tunable and selection-free gene expression in yeast. Sci. Rep. 7, 41431. https://doi.org/10.1038/srep41431.

Suzuki, R., Katayama, T., Kim, B.J., Wakagi, T., Shoun, H., Ashida, H., Yamamoto, K., Fushinobu, S., 2010. Crystal structures of phosphoketolase: thiamine diphosphate-dependent dehydration mechanism. J. Biol. Chem. 285, 34279–34287. https://doi.org/10.1074/jbc.M110.156281.

The_european_parliament_and_the_council_of_the_European_union, 2008. REGULATION (EC) No 1334/2008 OF THE EUROPEAN PARLIAMENT AND OF THE COUNCIL of 16 December 2008 on flavourings and certain food ingredients with flavouring properties for use in and on foods and amending Council Regulation (EEC) No 1601/91, Regulations (EC) No 2232/96 and (EC) No 110/2008 and Directive 2000/13/EC. Official Journal of the European Union L 354/34, 34–50.

Van Hoek, P., Van Dijken, J.P., Pronk, J.T., 1998. Effect of specific growth rate on fermentative capacity of baker's yeast. Appl. Environ. Microbiol. 64, 4226–4233.

Verduyn, C., Postma, E., Scheffers, W.A., Van Dijken, J.P., 1992. Effect of benzoic acid on metabolic fluxes in yeasts: a continuous-culture study on the regulation of respiration and alcoholic fermentation. Yeast 8, 501–517. https://doi.org/10.1002/yea.320080703.

Vuralhan, Z., Luttik, M.A., Tai, S.L., Boer, V.M., Morais, M.A., Schipper, D., Almering, M.J., Kotter, P., Dickinson, J.R., Daran, J.M., Pronk, J.T., 2005. Physiological characterization of the ARO10-dependent, broad-substrate-specificity 2-oxo acid decarboxylase activity of *Saccharomyces cerevisiae*. Appl. Environ. Microbiol. 71, 3276–3284. https://doi.org/10.1128/AEM.71.6.3276-3284.2005.

Vuralhan, Z., Morais, M.A., Tai, S.L., Piper, M.D., Pronk, J.T., 2003. Identification and characterization of phenylpyruvate decarboxylase genes in *Saccharomyces cerevisiae*. Appl. Environ. Microbiol. 69, 4534–4541. https://doi.org/10.1128/aem.69.8.4534-4541.2003.

Wang, Y., Zhang, H., Lu, X., Zong, H., Zhuge, B., 2019. Advances in 2-phenylethanol production from engineered microorganisms. Biotechnol. Adv. 37, 403–409. https://doi.org/10.1016/j.biotechadv.2019.02.005.

Wang, Z., Jiang, M., Guo, X., Liu, Z., He, X., 2018. Reconstruction of metabolic module with improved promoter strength increases the productivity of 2-phenylethanol in *Saccharomyces cerevisiae*. Microb. Cell Factories 17, 60. https://doi.org/10.1186/s12934-018-0907-x.

Wijsman, M., Swiat, M.A., Marques, W.L., Hettinga, J.K., van den Broek, M., Torre Cortes, P., Mans, R., Pronk, J.T., Daran, J.M., Daran-Lapujade, P., 2019. A toolkit for rapid CRISPR-SpCas9 assisted construction of hexose-transport-deficient *Saccharomyces cerevisiae* strains. FEMS Yeast Res. 19. https://doi.org/10.1093/femsyr/foy107.

Xu, P., Hua, D., Ma, C., 2007. Microbial transformation of propenylbenzenes for natural flavour production. Trends Biotechnol. 25, 571–576. https://doi.org/10.1016/j.tibtech.2007.08.011.

Zelle, R.M., Trueheart, J., Harrison, J.C., Pronk, J.T., van Maris, A.J., 2010. Phosphoenolpyruvate carboxykinase as the sole anaplerotic enzyme in *Saccharomyces cerevisiae*. Appl. Environ. Microbiol. 76, 5383–5389. https://doi.org/10.1128/AEM.01077-10.